REPUBLIC OF TURKEY

FIRAT UNIVERSITY

GRADUATE SCHOOL OF NATURAL AND APPLIED SCIENCES

TENSILE STRENGTH OF POLYCRYSTALLINE NiAl NANOWIRES: A MOLECULAR DYNAMICS STUDY

NYCHIR BAHRAM ABDULLAH

Master's Thesis

Department of Physics

Solid State Physics

Supervisor: Prof. Dr. Soner ÖZGEN

JANUARY, 2017

REPUBLIC OF TURKEY

FIRAT UNIVERSITY

GRADUATE SCHOOL OF NATURAL AND APPLIED SCIENCES

TENSILE STRENGTH OF POLYCRYSTALLINE NiAl NANOWIRES: A MOLECULAR DYNAMICS STUDY

NYCHIR BAHRAM ABDULLAH

Master's Thesis

Department of Physics

Solid State Physics

Supervisor: Prof. Dr. Soner ÖZGEN

JANUARY, 2017

REPUBLIC OF TURKEY
FIRAT UNIVERSITY
GRADUATE SCHOOL OF NATURAL AND APPLIED SCIENCES

TENSILE STRENGTH OF POLYCRYSTALLINE NiAl NANOWIRES: A MOLECULAR DYNAMICS STUDY

MASTER'S THESIS

Nychir Bahram ABDULLAH
(142114113)

Date of the Thesis submission to : 26th Dec. 2016
Date of Defense : 10th Jan. 2017

Supervisor: Prof. Dr. Soner ÖZGEN (Fırat University)

Assoc. Prof. Dr. Canan AKSU CANBAY (Fırat University)

Assis. Prof. Dr. F. Ahmet ÇELİK (Bitlis Eren University)

DEPARTMENT OF PHYSICS

Solid State Physics

ELAZIG

ACKNOWLEDGMENTS

First of all, I would like to thank Allah for giving me the strength and courage to complete my master's thesis. I would like to express my special thanks to my supervisor, Prof. Dr. Soner Ozgen. Without him, it would be impossible for me to complete this thesis.

I am indebted to my mother and father, brothers, sisters, my lovely wife and all my friends who encouraged me to complete my master degree with their continuous support during my studies. Finally, I want to say thanks to everyone that help me to prepare a final thesis.

Nychir Bahram ABDULLAH
Elazığ-2017, TÜRKİYE

In this thesis, High Performance and Grid Computing Center resources (TRUBA-TRGRID) provided by ULAKBIM (Turkish National Academic Network and Information Center) were partially utilized in order to run simulation codes.

CONTENTS

Pages

SUMMARY

In this thesis, polycrystalline nanowire models of NiAl alloy were created and the stress-strain behavior of these models was investigated by using the molecular dynamic simulations. For this purpose, physical interactions between atoms are modeled by the embedded atom method and simulations are performed with open source code LAMMPS package.

A total of six different models with square-shaped in size of $2x2nm^2$, $3x3nm^2$, $4x4nm^2$, $5x5nm^2$, $6x6nm^2$, and $7x7nm^2$ and 10nm length were prepared. Also, each model has been replicated to contain four different numbers of grains, but the almost same shaped. The number of grains in the models are 2, 3, 4, and 5. Thus, while at least the small model contains 3100 atoms, the largest model contains 40000 atoms. The prepared models were first thermodynamically relaxed at 300K temperature for 20000 time steps each of 2fs. and settled in stable structures. Then, on the model nanowires, tensile forces were applied in the *z* direction with a speed of 1m/s strain until the fracture point. In this process, thermodynamic, mechanical and structural properties of the models have been determined by performing molecular dynamic calculations. From the obtained results, Young modules and yield strengths of nanowires were calculated from the stress-strain curves. The results are discussed in comparison with the literature.

Keywords: Nanowires, NiAl alloys, Molecular Dynamic Simulation, Mechanical Properties, Stress-Strain Behavior.

ÖZET

POLİKRİSTAL NİAL NANOTELLERİN GERİLME DAYANIMLARI: MOLEKÜLER DİNAMİK ÇALIŞMASI

T.C. Fırat Üniversitesi, Fen Bilimleri Enstitüsü, 46 Sayfa.

Bu tezde, NiAl alaşımının nano ölçekli tel modelleri oluşturulmuş ve bu modellerin moleküler dinamik simülasyonları yardımıyla zor-zorlanma davranışları incelenmiştir. Bu amaçla, atomlararası fiziksel etkileşmeler gömülü atom metodu ile modelllenmiş ve simülasyonlar açık kaynak kodlu LAMMPS kodları ile gerçekleştirilmiştir.

Kare taban şekilli 2x2nm^2, 3x3nm^2, 4x4nm^2, 5x5nm^2, 6x6nm^2 ve 7x7nm^2 boyutlarında ve 10nm uzunluğunda toplam altı farklı model hazırlandı. Ayrıca, her model dört farklı grain içerecek şekilde çoğaltıldı, fakat tane şekillerinin hemen hemen aynı kalmasına özen gösterildi. Modellerdeki tanelerin sayısı 2, 3, 4 ve 5 dir. Dolayısıyla, en küçük model 3100 atom içerirken, en büyük model 40000 atom içerir. Hazırlanan modeller, ilk önce, her birisi 2fs olan toplam 20000 zaman adımı boyunca 300K sıcaklıkta termodinamik olarak dengelendiler ve kararlı yapılarına yerleşmeleri sağlandı. Daha sonra, model nanotellerde, kırılma noktasına kadar 1m/s hızla z yönünde gerilme kuvveti uygulandı. Bu süreçte modellerin termodinamik, mekanik ve yapısal özellikleri moleküler dinamik hesaplamalar yapılarak belirlendi. Elde edilen sonuçlar doğrultusunda, zor-zorlanma eğrilerinden Young modülleri ve nanotellerin akma mukavemetleri belirlendi. Sonuçlar literatür ile karşılaştırılarak tartışıldı.

Anahtar Kelimeler: Nano Teller, NiAl alaşımı, Şekil Hafızalı Alaşımlar, Moleküler Dinamik Simülasyonu, Mekanik Özellikler, Zor-Zorlanma

LIST OF FIGURES

Pages

LIST OF TABLES

Pages

ABBREVIATIONS

A : Area

BCC : Body Centered Cubic

d : Grain size

E : Young's modulus

E_{tot} : Total energy

EAM : Embedde Atom Method

F : Force

FCC : Face Centered Cubic

G : Grain

G2 : 2 grained model

G3 : 3 grained model

G4 : 4 grained model

G5 : 5 grained model

GB : Grain Boundary

GPU : Graphical Processor Unit

HCP : Hexagonal Closed Packed

k : Grain constant

LAMMPS : Large-scale Atomic/Molecular Massively Parallel Simulator

LATGEN : Lattice Generator Code

m_i : Atomic mass of atom *i*

MD : Molecular Dynamics

MEAM: Modified Embedded Atom Method

MEMS: Microelectromechanical System

NEMS: Nanoelectromechanical System

NiAl : Nickel-Aluminium

SMA : Shape Memory Alloy

Q-SC : Quantum Sutton Chen

TB : Twin Boundary

Voro++ : Voronoi tessellation library

σ_y : Yield stress

σ_o : Bulk yield stress

1. INTRODUCTION

Today, when nanotechnology is being used in our everyday life, the scientific and engineering work done in this area is rapidly increasing. Nanotechnology can be defined as the most important technology of the century and most of the countries make significant investments in this technology nowadays. A pretty understanding of properties of the nanostructures can contribute to both the development of nanotechnology and the usage of them in daily life. By structure, the research fields on nanoscale materials are classified as nanocrystals, nanoparticles, nanotubes, nanowires, nanorods or nanoscale thin films. These structures have many amazing physical behaviors that are not yet fully understood in atomic level. Therefore, the explorations on these material behaviors in nanoscale have been continued by theoretical and experimental studies [1].

Nanowires are defined as rod-like materials with diameters in the range of 5-100nm. They are often made from metals or semiconducting materials as well as metal alloys in order to use in nanoelectromechanical system (NEMS), which they are typically integrated transistor-like nanoelectronics devices. Also, they can be used as mechanical actuators, pumps, or motors as well as physical, biological, and chemical sensors in MEMS devices [2]. Researches on nanowires is often conducted along with the research on carbon nanotubes which they are attributed to as a probe material in nanoscience. Metals and semiconductor nanowires exhibit unique electrical, mechanical, magnetic, optical or thermoelectric properties, when compared to their bulk counterparts. Especially in sensor applications, the great effort is being made on the nanowires due to their large surface/ volume ratio which gives a prospect for high sensitivity. On the other hand, one of the most important things that should be well known in the application of metal nanowires is their elastic behaviors during tensile loading applications [1-5]. Due to the increasing surface/volume ratio, the interatomic interactions on the surfaces are stronger, and consequently the increased surface tension and energy can alter some mechanical properties of these materials. In this case, the physical laws governing the macroscopic behaviors of the materials may be changed more or less for the nano-sized materials. Thus, it is necessary to determine whether there is a change or not in mechanical rules. In these researches, it is also important if the material of interest is formed in single crystal or polycrystalline states.

Perhaps the most important parameters on the mechanical properties of solids are those that relate to flexibility and durability. Upon mentioning elastic properties of materials, the Young's modulus, yield strength, ultimate strength, and fracture point are the parameters, which are generally determined by tensile tests [6, 7]. It is relatively easy to conduct these experiments on macroscopic scale. However, it is difficult to carry out these experiments when the size of materials are decreased. Nano- and even pico-sized indentation experiments can be performed instead of the conventional tensile tests [1, 8-13]. Another method uses resonant techniques [8, 9, 11]. In these techniques, nanoscale material is vibrated by the help of electric or magnetic fields. Then, the natural frequencies of the materials are determined by transition or scanning electron microscopy. As a result of calculations using these frequencies, the elasticity modules of the nanoscale material are obtained [14-16]. Experimental results have shown that the Young's modulus of the nano-tellurium increases rapidly with decreasing wire diameter, especially below 100 nm [17-21]. In the light of this result, it is understood that there is no enough atomic layer that can cause strain slipping, which is the cause of plastic behavior with shrinking dimensions, and that internal constraints cannot be produced to get an inappropriate misfit, structural dislocations [22-24]. In addition, most of the plasticity theory take into account the surface effects of the material and show that surface effects are important even for macroscopic materials [1, 25, 26]. From this point of view, the results reveal that the magnitude of surface energies can significantly change the mechanical parameters of materials.

In generally, many metal and alloy materials have been produced by solidifying from liquid states, in the case of desiring low cost of production. Microstructural properties of these materials depend strongly on the cooling rate. The materials solidified at very low cooling rates have usually crystal structures whose atoms are located at certain lattice points in the space. However, as increasing in cooling rate the atoms cannot find enough time to settle in the ordered points, resulting in different microstructures such as amorphous, or polycrystalline states. Even for at low cooling rates, if the crystallization begins at different parts of materials, especially homogenous nucleation of new solid phase inside of the liquid, different oriented crystalline regions can occur in the materials. As these crystalline regions grow, they finally hit each other by constraining themselves at their boundaries and by forming the grains. These grains affect the material properties related with thermodynamics, mechanics and electric, depending on grain size and shape, the number of grains, crystal

orientations in the grains, and their boundary structures. Although there are many theories to explain how these parameters relate to the grain properties in macroscopic state, but a few in nanoscale. In this case, there is something new to explore.

In many cases, experimental studies in nano scale are very difficult and require a lot of time consuming processes. Instead of this experimental studies, sometimes scientist use computer simulations which they are useful to make a bridge between theory and experiments. One of the widely used simulation approaches is molecular dynamics (MD) simulation. In this technique, it has been aimed to get the minimum energy point in the phase space of the modeled physical system by using the numerical integration of the equations of motion derived from the mechanical Lagrangian or Hamiltonian functions [27]. It has been observed that the simulation results are very close to the results from real experiments when the appropriate models are used. In this calculations, potential energy functions defining the interatomic interactions, play an important role to obtain suitable data [28]. There are various computer programs and open source codes developed for MD simulations [29]. Some of these codes can be found as an open-source form on the internet resources and they are widely used under the GNU license; LAMMPS (Large-scale Atomic / Molecular Massively Parallel Simulator) [30], GROMACS [31], IMD [32] and NAMD [33]. Also, these software use parallel computing technique and can be used to study molecular systems consisting of several million atoms [1].

The physical interactions between atoms in metals and alloys can be modeled conveniently by using potential energy functions in the concept of many-body interactions. The most commonly used potential energy approach for many-body interactions is known as the embedded atom method (EAM) [34]. In the concept of EAM, the potential energy of an atom in a crystal is expressed as the sum of electrostatic repulsive energies and the sum of embedding energies which define the attracting interactions raising from electronic charge density in the atomic location. The most common types of EAM approach to model NiAl alloys are Voter-Chen [VC], Sutton-Chen [SC], and the last EAM approach developed by PurjaPun and Mishin [35, 36].

By using MD simulations the yield strength of Ni and Cu nanowires depending on wire thickness and crystal orientation was determined by Yang et al. [37]. In that study, the researchers used the MEAM (Modified EAM) approach to model the interatomic interactions, developed by Baskes [38]. They also used rectangular structures with square

cross-section and in dimensions of 40 lattice spacing in z direction and 6-10 in xy direction as a model system. Nose-Hoover thermostat was applied for 50 ps at 300 K temperature in order to get thermal equilibration of models. The integration step size was selected as 2 fs. One ends of the model wires was fixed and pulled at the other ends at specific speeds. All of the MD simulations were done by using LAMMPS. From the results, it was determined that the decreasing in nanowire cross-section area gives rise to increase in the flow stress [1].

Çağın et al. [39] used a Q-SC type EAM model to perform a stress-strain test on the CuNi alloy nanowires. Plastic deformation of the model systems with a thickness of 2 nm was investigated in their study. They used various speed of stress application from 0.005 to 0.05 ps^{-1}. From the results, they reported that, due to the small thickness of the nanowire models, sufficient plastic deformation could not be formed in the system, but instead, successive multi-twinning-type deformations formed, which harden the nanowires. They also reported that the increasing the strain rate reduced the magnitude of twinning, and at higher rates of stress a certain amorphization of structure was observed [1].

A study on the deformation of FCC nanowires by twinning and slip mechanisms was done by Park et al. [40]. In that study, the researchers performed the MD simulations to analyze the deformation of single crystal metal nanowires for copper, nickel and gold, with various crystallographic orientations loaded in tension and compression. To model the interatomic interactions of the materials they used different EAM approach since the stacking fault energies are needed to calculate accurately. Their nanowire models had a square cross section and they were created by extracting from a bulk FCC crystal. The wire lengths were all 40 cubic lattice units in the *x*-direction, with cross sectional lengths of six cubic lattice units in the y- and z-directions. Nose-Hoover thermostat was applied for 20ps at 50K for gold model and 300K temperature for copper and nickel systems in order to get thermal equilibration.

Huang et al. [41] studied on the strain rate and size effects on mechanical properties of FCC nickel nanowires by using MD simulations based on modified EAM developed by Baskes [38]. In that study, by applying the periodic boundary conditions only in the *z* direction, an infinitely long nickel nanowire was constructed as a model system with square cross section on the plane *x*-*y*. Also, the periodic boundary condition was not applied in the other two directions, *x* and *y*. To obtain an initial equilibrated structure of nickel nanowire, the model were relaxed for 100ps, by running 50,000 steps, each of 2fs. The system

temperature was fixed to 300K by using Nose–Hoover thermostat, and the Berendsen barostat algorithm was used to control the system stress. At the end of the study, the researchers obtained a stress-strain curve similar to that of the conventional tensile tests of macroscopic materials, and they characterized the stress-strain curve into three period identical to that of conventional polycrystalline metals: an initial elastic period, a yielding period, and a hardening and failure period. They found that the yielding strain of nanowires is independent of both the strain rate and cross-sectional size [41].

In this thesis, the stress-strain relations of polycrystalline Ni-at.50%Al alloy nanowires was investigated by using MD simulations, depending on the nanowire thickness and the number of grains inside of the model system. For this purpose, LAMMPS package [30] was used to integrate the equation of motion of the model systems. The EAM approach developed by PurjaPun and Mishin [36] was preferred to describe the interatomic interactions, due to the best matching its stacking fault energy with experiments. Grain structures were constructed with the help of LATGEN (LATtice GENerator) package [42] which has distributed under GNU license, and the initial atomic coordinates inside of these grains were set up on the B2 superlattice points having random crystal orientations in each grain. In this manner, 6 different thicknesses and 4 different number of grained systems were produced. The nanowire models were stretched using only one stress rate and then stress-strain curves were plotted. From the strain-strain curves, the Young's modules and flow stress values of the nanowire models were determined. Dependency of these parameters on model thickness and number of grains were investigated. The structural evaluation of models under tensile loading and their relations to the size and number of grains were estimated.

2. TENSILE BEHAVIOUR OF METALLIC MATERIALS

2.1. Stress-Strain Curves

Every solid are flexible up to certain extent. To determine a group of terms for which a force is applied to a solid object, the applied force will lead a small shift in the shape and the volume of the object, due to its torsion, pulling or compressing, when the applied force is removed on the body it will return to its original shape. The distortion force (*F*) per unit area (*A*) is called stress and it is calculated as *F*/*A*. This stress that can be applied in the form of tensile or compression, produce strain on the rod-shaped solid objects. The strain produced by tensile stress can be calculated by ($\Delta l/l$), so it is a unitless quantity [43]. When the tensile stress is applied on the material, the change in the length of rod-shaped material can be shown in Figure 2.1 (a), and as a general example for the stress-strain relation during the tensile loading can be shown in Figure 2.1 (b).

According to the elasticity theory of the materials, the strain is proportional with the applied stress within the first and small portion of the stress-strain curve and the constant of proportionality is called as Young's modulus (*E*) or modulus of elasticity, the slop of the curve [43]. The Young's modulus is defined mathematically as:

$$F/A = E(\Delta l/l) \qquad 2.1$$

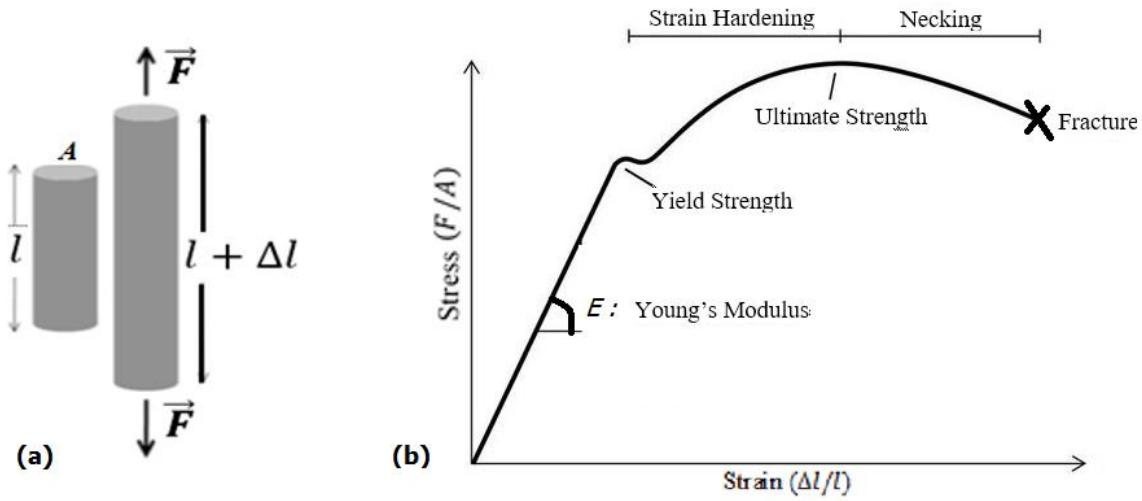

Figure 2.1 (**a)** A rod-shaped material under tensile stress and (**b)** a typical stress–strain curve.

As shown in Figure 2.1 (b), the strain–stress curve consists of two parts: The first one is defined as the elastic behavior region where stress and strain are dependent linearly on each other. In this part, the material can return to its original shape after removing the applied tensile stress. In the second part is defined as plastic behavior region where the sample is deformed irreversibly, and consist of two sub-region: Strain hardening and necking. At the end of the necking region the fracture is observed.

At the point of changing elastic behavior to plastic behavior region, the value of the stress is defined as yield stress. If the stress value is higher than the yield stress point, the crystal lattice of the sample will be unstable and no longer can exhibit the elasticity behavior. The perfect strength of a metals can be specified as the critical stress, when the crystal is in the ideal case, free of defects, and under regular distortion [44]. In some cases, the yield of bulk material begins at a stress less than its perfect strength, this is accompanied generally with the defects occurring in the lattice, such as grain boundaries and dislocations.

Strain hardening, also known as work hardening occurs especially when the temperature of the material is much less than its melting point and the applied stress is higher than the yield stress point. To produce more plastic deformation, the stress should increase above the yield point. Hence the deformation of the material will be too difficult because it is hardened. Work, or strain, hardening can be interpreted as the plastic deformation related with the multiplication and movement of a big number of dislocations inside the crystal structure. When plastic deformation process occurs, the reciprocal space among dislocations decline and they start forming dislocation junctions, because they are blocking the movement of each other (this technique can be termed as dislocation forest hardening), and then at grain boundaries they start piling up. After this stage, in order to make an extra plastic deformation a higher stress is required. Normally, the stress-strain curve is drawn in terms of engineering strain and engineering stress, in the other word the strain and stress are measured according to the original dimensions of the material and not according its values during the measurement. From the previous concept the ductility of the materials can be defined. Ductility is the capacity of the materials undergoing a plastic deformation and it is an important parameter in the material science. The plastic deformation mechanism of materials depends on the microstructural properties of the interested materials such as defect structures or grain properties [44].

2.2. Grains and Polycrystalline Alloys

Grains are identified as a group of neighboring atoms in the same crystallographic orientation (Figure 2.2). Grain boundaries are the disordered region between two unique grain orientations. Grain boundaries are less dense than the crystalline grains and store free volume throughout the boundary [45]. Atoms in grain boundaries have higher energies than perfect crystalline atoms therefore they are not in the energetically favorable locations. Also, in some solid-solid phase transformations, especially shown in shape memory alloys like NiAl alloys having special composition range which exhibit thermoelastic martensitic phase transformations, these atomic movement for getting the favorable states are held responsible for starting the structural transformations [46]. Consequently, research on the tensile strength of grained shape memory alloys became valuable in technological applications [47].

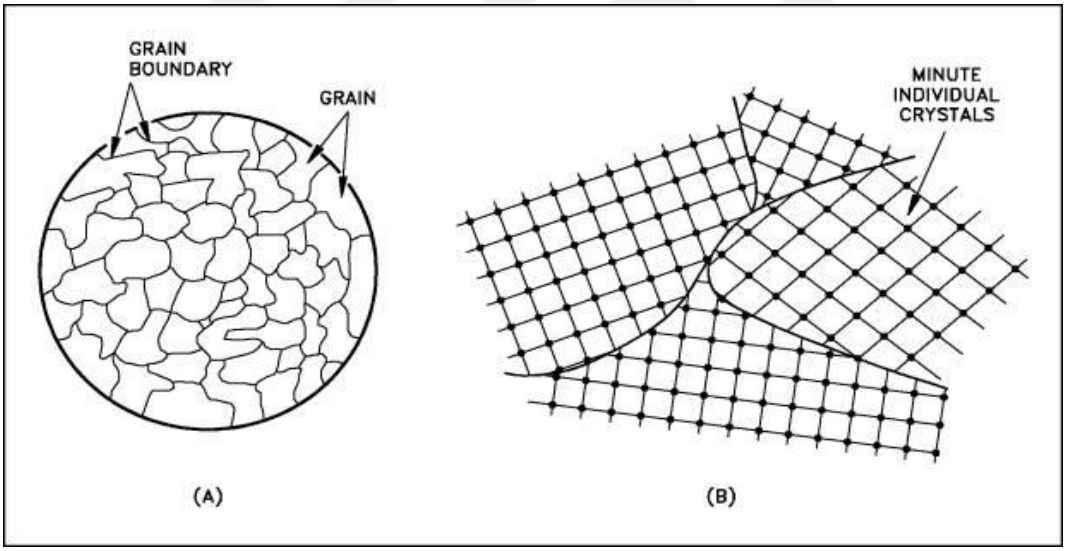

Figure 2.2 (a) Grain formation in a metal and (**b)** grain orientations.

2.3. Defects in Metals and Alloys

Inside the metallic alloys and solid metals, the atoms are sorted in a regular pattern in the shape of crystal. In a lattice the atoms are sorted and repeated periodically. In this cases the structure is defined as the crystal structure. The more significant structures are the hexagonal

closed packed (HCP), the face centered cubic (FCC) and the body centered cubic (BCC), which they are shown in Figure 2.3.

Generally, the repetition of the crystal structures is not ideal due to some deformation is occurred inside the lattice by several defects. Mechanical properties of solid materials depend mainly on the defects and also it takes responsibility of macroscopic behavior for the solid materials, especially when the external stress are applied on the materials. For this reason, the defects are very important in material sciences [48].

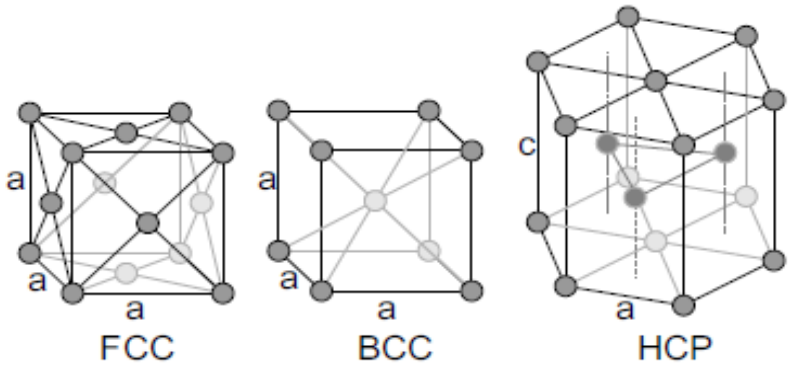

Figure 2.3. Common lattice structures in solid metals [48].

Crystalline defects can be classified according to its dimensions:

Point Defects - (0.D): When one of the atoms is not found at its regular location, i.e. it found outside of its ideal lattice position, in this case the defect is called self-interstitial. This kind of defect is not common in solid metals, as high energy needed to produce an interstitial defect. In case where an atom is lost in the lattice, the defect is called a vacancy. Also impurity atoms are another reason to form point defects. May this atoms form interstitial in the lattice, or they can be substitute atoms in the lattice.

Line Defects - (1.D): Line defects is the line of dislocated atoms, so they are called as dislocations. The ductility and strength of materials depend substantially on the line defects. Also, in the case of plastic deformation of materials, the movement of dislocations in crystalline solids is the dominant mechanism. In general, there are two type of dislocations in this manner, edge and screw dislocations as shown in Figure 2.4.

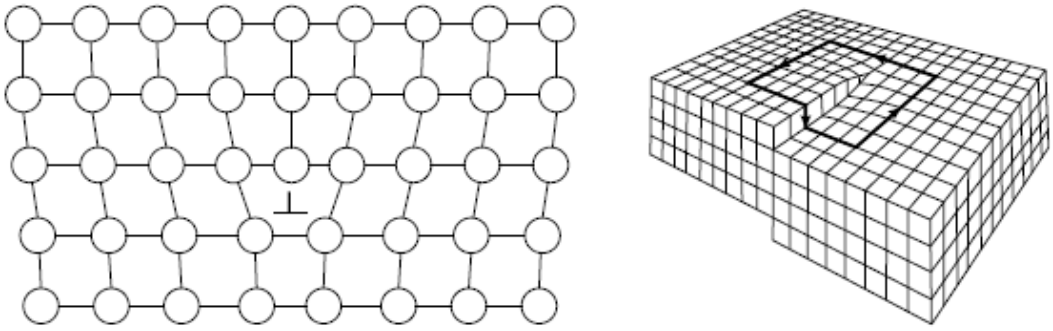

(a) **(b)**

Figure 2.4. Two main types of 1.D dislocations in a simple cubic lattice. **(a)** Edge dislocation and **(b)** screw dislocation [51].

The screw dislocations are created when the crystal being shifted and cut by one atomic spacing or by shearing the lattice. The motion of the screw dislocation or line defect is perpendicular to direction of the applied stress.

Surface Defects - (2.D): There are a large number of grains or crystals inside crystalline solids, because the majority of crystalline solids are polycrystals. The orientations of the lattice inside each grain is different from the neighboring grains. In crystalline solids the grains are separated by the grain boundaries and they are interfaces between the adjacent grains. In each grain the atoms which lie on the boundaries have mismatch orientation with the atoms of neighboring grain, as shown in Figure 2.5.

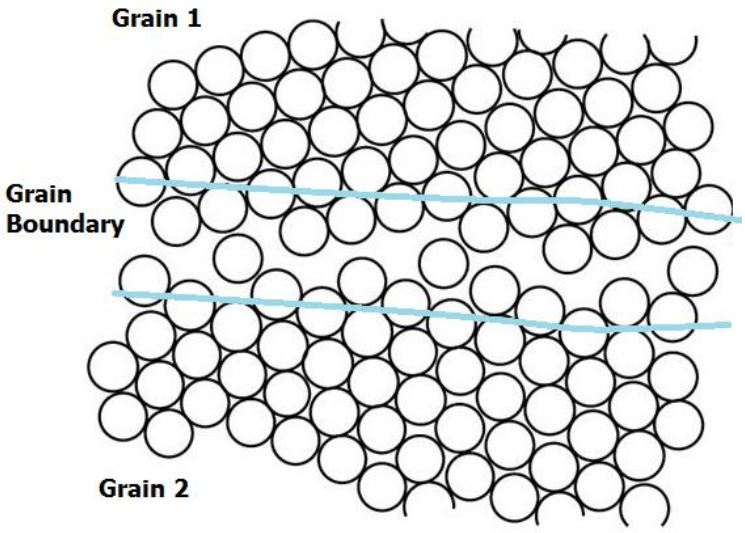

Figure 2.5. The orientation of the atoms in the grains and grain boundary structure.

When the misalignment angle is small, less than ten degrees, it is termed low angle grain boundary, and if it is greater than fifteen degrees it is called high angle grain boundary as shown in Figure 2.6. If the low grain boundary is created by the screw dislocations it is called twist boundary, and if the boundary is formed by edge dislocations then it is called as tilt boundary [49, 50]. As we mentioned before at the grain boundary the atoms have disordered orientations, but crystalline solids are remain extremely strong, because of the presence of the cohesive forces across and within the boundary.

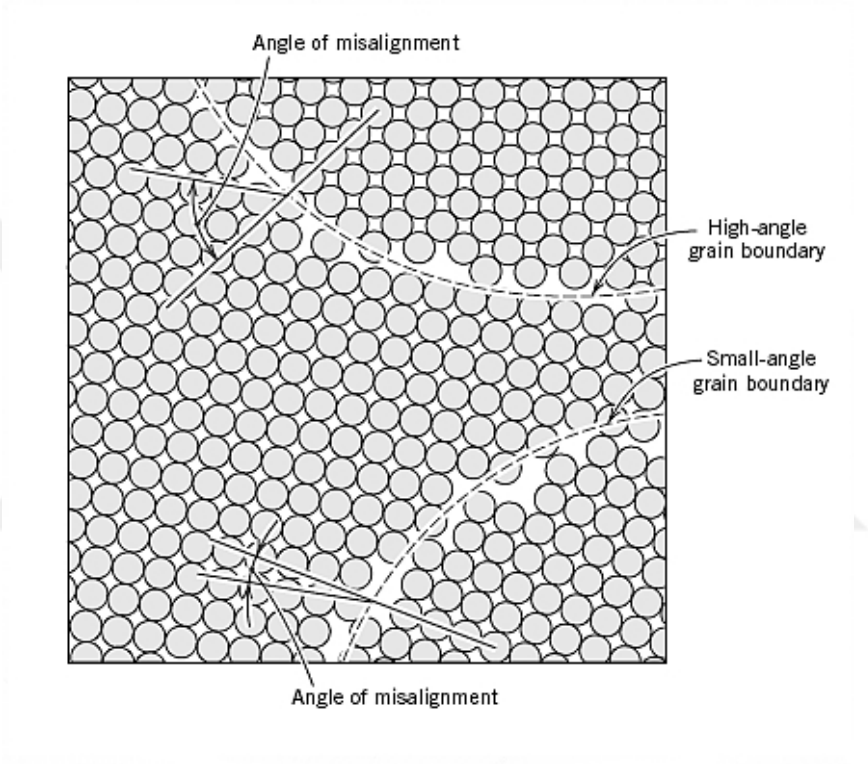

Figure 2.6. The misalignment angle of the grains [52].

2.4. Tensile Behavior of Metal Nanowires

One of the most important properties of metal nanowires is their elastic behaviors during tensile application namely, the stress-strain relationship. From the Hall-Petch relation, it has been understood that the yield strength σ_y of grained structures increases as decreasing in the grain size as shown in Figure 2.7. Then, it was considered that if grain size could be decreased even further to the nano-scale the yield strength would increase well. Nevertheless, experiments on many nano-crystalline materials exhibited that if the grains reached a small enough size, the crystal grain size which is typically around 10nm [53-60],

the yield strength would either remain constant or decreases which decreasing grain size because grains are unable to support dislocation pile-ups. This phenomenon is called as the inverse Hall-patch relation as shown in Figure 2.8. Several mechanisms have been proposed to explain this relation: i-dislocation-based [54, 55], ii- diffusion-based [56, 58], iii- grain boundary shearing-based [59-62], iv- two phase-based [63-65]. The pile-up of dislocation near grain boundary is an important mechanism of the Hall-petch relationship. Once grain size drop below the equilibrium distance between dislocations, though, this relationship should no longer be valid. Nevertheless, it is not entirely clear what exactly the dependence of yield stress should be on grain size below this point.

The equation of Hall-Petch [64] is given by:

$$\sigma_y = \sigma_0 + kd^n \tag{2.2}$$

In Eq. (2.2), σ_0 is the materials yield strength or (friction stress in the absence of grain boundaries) at the bulk scale, *d* is the grain size. The terms *n* and *k* are the constants of the related material. Generally, *n* is about -0.5, but it may change significantly from -0.5 to -1.

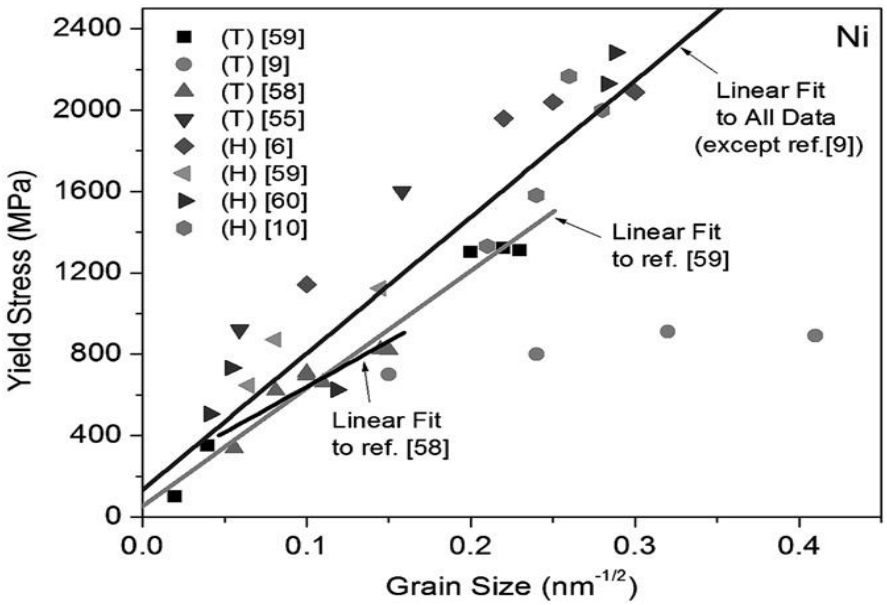

Figure 2.7 Hall–Petch relationship for Ni determined by several research works. T Denotes tensile tests and H denotes hardness tests [64].

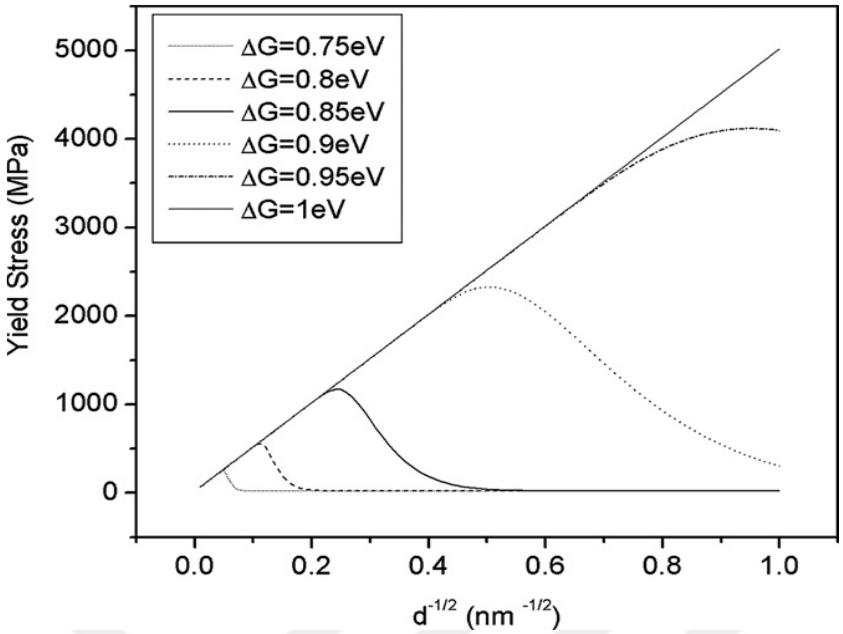

Figure 2.8 The modified Hall–Petch relationship for Ni deformed under a strain rate of 10^{-5} s^{-1} at 293 K, showing the inverse Hall–Petch [64].

In fact, there are several mechanisms contribute in the plastic deformation of metal nanowires, every mechanism depends on the several factors like aspect ratio of the material, kind of the mechanism test, and also initial defects of materials. Main reasons of the plastic deformation are the multiplication of dislocation in the material, by diffusion or nucleation. As mentioned before it has been observed when the grain size decrease the strength of the nanocrystalline materials increase, because the dislocation cannot diffuse freely due to the presence of a big number of two dimensional barriers, for example pile up faults, grains and interface boundaries [66]. When the domain size become smaller, the dislocations faced with more barrier during diffusion so that they are more likely undergo piling up at that barrier, before the dislocations can multiply. Hence, in the other side of the boundary the dislocations can be nucleated as increasing the accumulation of stress on opposite. Then the stress release at the boundary. The mechanism that blocking the motion of dislocations, also reduces the ductility of the nanomaterials [67].

In this field, densely scientific researches have been carried out because it would be very great to have nanocomposite materials having improved ductility and strength. Modern researches have been explained that precision engineered coherent internal boundaries in nanomaterial could realize this target [67]. That mutual strengthening of materials depends on the grain boundary engineering. However, grain boundaries are incoherent, i.e. there are no any relationships between the grains because at the boundary there are many broken

atomic bonds and voids. Grains own have very high energy, and interfaces between the grains can rupture and deform by high extra stress. For this reason the grains have fixed capability to absorb the dislocations before deforming. On the other hand, coherent internal boundaries own have very small energy and among them twin boundaries have a good mechanical and thermal stability.

Twin boundaries progress with extra way for dislocations to diffuse and allow the dislocations to propagate through them so that the dislocations can glide down along a twin boundary. Common interface along the boundary makes nanomaterial to undergo enough shear deformation among the twin boundaries without any splitting, as seen in Figure 2.9 [67]. It has been revealed by the scientific researches, when the twin thickness become smaller, the ductility and strength of the material will increase.

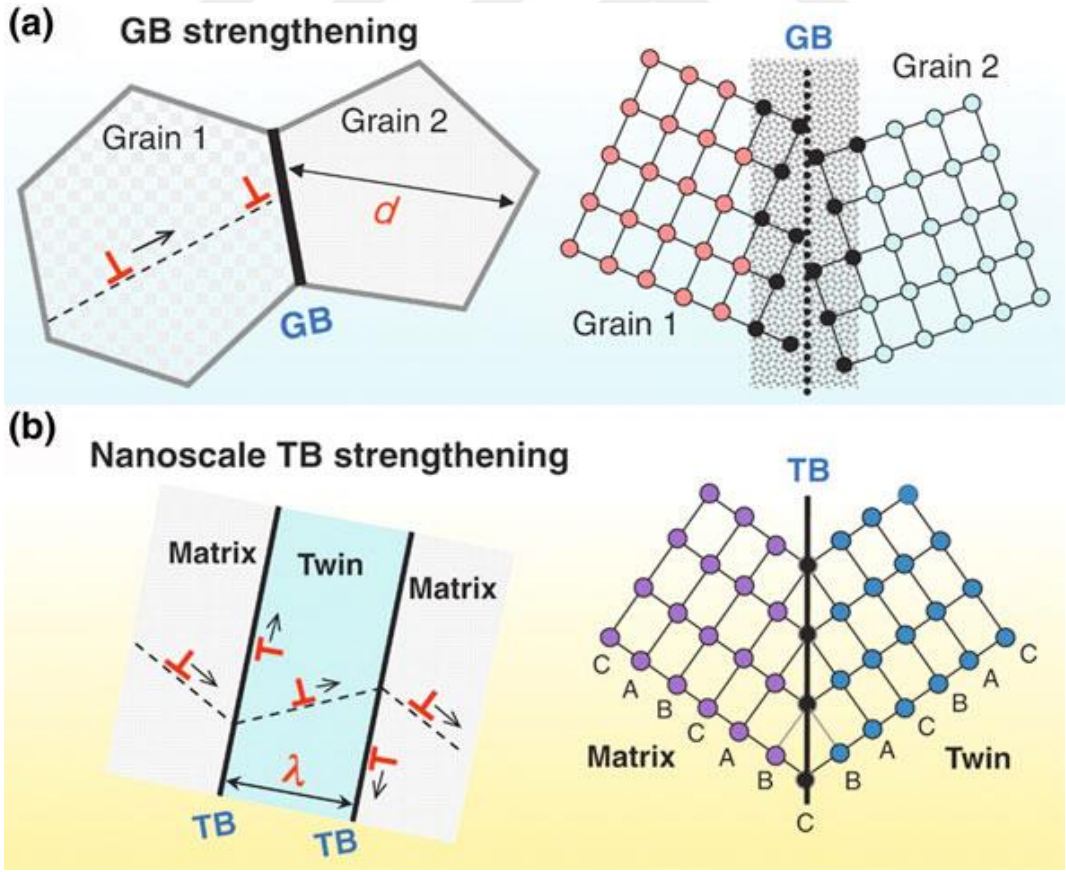

Figure 2.9. **(a)** The propagation of a dislocation stops at a grain boundary. **(b)** The dislocation sliding along the twin plane [67].

2.5. Mechanical Properties of Polycrystalline NiAl Alloys

Intermetallic compound of NiAl with B2 crystal structure is regarded as a potential candidate of high temperature structural materials because it offers a wide range of attractive mechanical, chemical and physical properties, such as high melting point, low density, good thermal conductivity and high stiffness [68]. However, it exhibits inherently brittle fracture and zero ductility at ambient temperatures, and its use as engineering materials is restricted in many cases by its poor fracture resistance and limited fabricability. In an attempt to improve the ductility of single phase NiAl, the tensile behavior of NiAl has been investigated at wide ranges of temperatures and strain rates using polycrystals and single crystals. In addition, the deformation of NiAl by compression has been studied. Some interesting results were disclosed by these studies. For NiAl single crystals with various kinds of orientation, the anomalously large tensile elongation like almost the superplastic deformation has been observed to take place at a very limited temperature regime of 0.35~0.40 T_m. For NiAl polycrystals, extruded NiAl underwent obvious a brittle to ductile transition at about 400℃ and exhibited superplasticity at temperatures ranging from 1000℃ to 1100℃ under initial strain rates of 1.67×10^{-4}~1.67×10^{-2} s^{-1}. There were substantial evidences indicating that details of the dislocation structure play a central role in determining the deformation behavior of NiAl. At room temperature and below NiAl deformed almost exclusively by the motion of <100> dislocations whose Burgers vector gives only three independent slip systems. At intermediate temperatures, where a brittle to ductile transition occurred, <110> dislocations began to contribute to the plastic deformation. The superplasticity observed at high temperatures [68].

2.6. Stress-Strain Behavior of NiAl Alloys

The deformation behavior of the alloy true stress versus true strain curves has been seen in Figure 2.10, which were plotted on the assumption of uniform deformation strain [68]. Figure 2.10 (a) illustrates the true stress versus true strain curves of NiAl deformed at different strain rates at 1373 K. It clearly shows that at high strain rates, the true stress–true strain curves exhibit a continuous increase of stress up to high strain (0.60), followed by a relatively rapid decrease of stress. At the lower strain rates, the flow stress decreases and the strain of steady flow increases. The extended steady flow behavior indicated uniform plastic deformation up to large strains without fracturing and therefore good necking resistance of

the tested specimens. The influence of temperature was similar to that of the influence of strain rate; an increase in temperature led to the same pattern in the true stress–true strain curves as that observed by a decrease of strain rate, Figure 2.10 (b) [68].

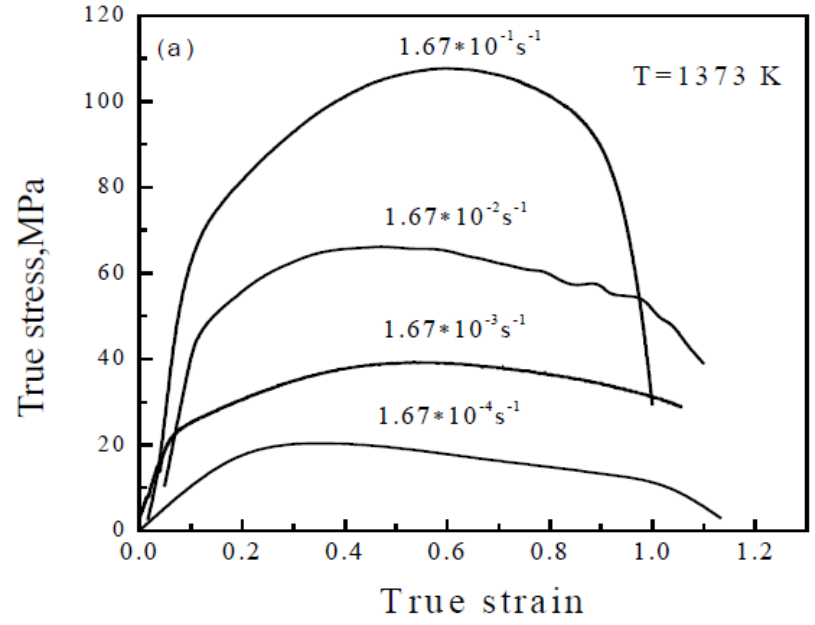

(a)

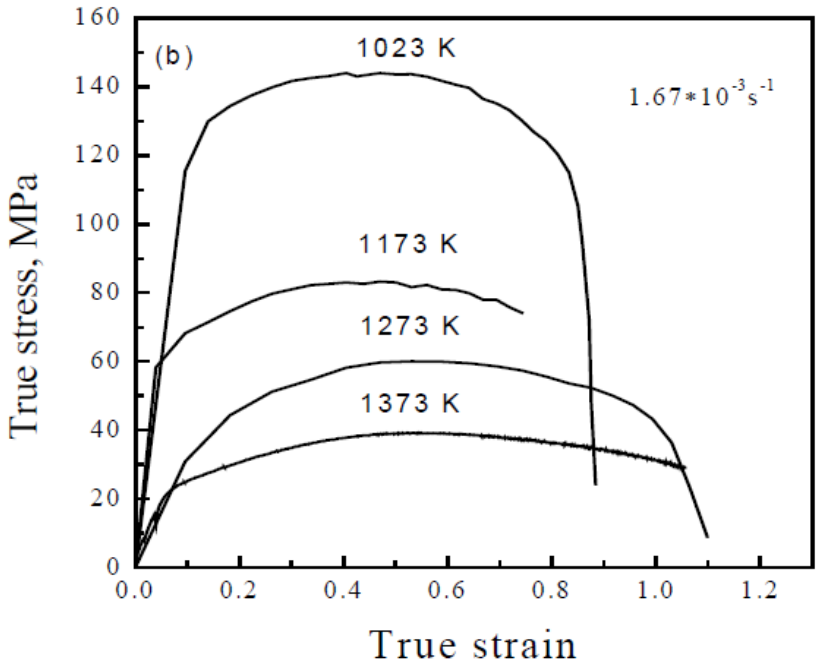

(b)

Figure 2.10. Stress-strain curves of NiAl alloys at different (**a**) strain rates and (**b**) temperatures [68].

3. MOLECULAR DYNAMICS CALCULATIONS

Molecular dynamics simulations serve as a good bridge between experimental work and theoretical work. Basically, physical interactions between atoms are defined by potential energy functions, and the equations of motion of the system are integrated by numerical methods, using suitable algorithms. Thus, by calculating the time-dependent positions and velocities of atoms, the model system achieves minimum energy structure in phase space, i.e. equilibrated structure, making it possible to study the behavior of physical model systems that are difficult to observe experimentally [69-72].

MD calculations are usually planned in three parts: *i*- initialization, *ii*- equilibration and *iii*- production [69]. In the first part, the equations of motion of the system is formed as an initial value problem and then the initial positions and velocities of the atoms in the system are defined as the initial conditions of the system. In the second part, the equations of motion are solved by using numerical integration algorithms and the system is forced to move to a minimum energy position in the phase space, as a thermodynamic condition of the system. In the third part, the results are obtained by making various physical measurements (calculations) on the system in the thermodynamically equilibrated state. One of the key factors in achieving the correct results from the simulations is the selection of potential energy functions suitable for the physical interactions between the atoms [1, 70, 71].

In the MD method, various constraints are introduced on some thermodynamic variables in order to obtain the equations of motion of the physical system. For an example, if a physical system has the constant number of particles (*N*), constant volume (*V*), and constant total energy (*E*) then the system is called as '*NVE* statistical ensemble'. As a different model system established for the constant number of particle, constant pressure (*P*) and constant enthalpy (*H*) are known as the *NPH* statistical ensemble [70, 71]. For the systems where the temperature (*T*) is constant, the *NPT* and *NVT* statistical ensembles can be given as another examples [1].

3.1. Molecular Dynamics Method for *NVE* Ensemble

The Lagrange function of the system (*NVE* ensemble) with the potential energy function between the atoms, $\Phi(r_{ij})$, can be defined as follows:

$$L = \frac{1}{2}\sum_{i=1}^{N} m_i \dot{r}_i^2 + \sum_{i=1}^{N-1}\sum_{j>1}^{N} \Phi\left(r_{ij}\right) \tag{3.1}$$

In here, the velocity of the particle *i* is $\dot{r}_i$, $r_{ij} = |\boldsymbol{r}_{ij}| = |\boldsymbol{r}_i - \boldsymbol{r}_j|$ is the distance between particles *i* and *j*. By solving the Lagrange function above, the equation of motion of the particle *i* is obtained as:

$$m_i \ddot{r}_i = F_i = -\sum_{j\neq i}^{N} \frac{\partial \Phi(r_{ij})}{\partial r_i} \hat{r}_{ij} \tag{3.2}$$

Here m_i is the mass and $\ddot{r}_i$ is the acceleration of the particle *i*, and $\hat{r}_{ij}$ is $\boldsymbol{r}_i - \boldsymbol{r}_j$ represent the vector difference between the positions of atoms *i* and *j*.

A numerical solution can be made after the equations of motion of a system are obtained. In numerical solutions, various algorithms such as Euler, Runga-Kutta, Gear and Verlet are used [1, 69, 70]. The most preferred algorithm is the velocity form of the Verlet algorithm:

$$x_i^{n+1} = x_i^n + h v_{ix}^n + \frac{h^2}{2m_i} F_{ix}^n \tag{3.3}$$

$$v_{ix}^{n+1} = v_{ix}^n + \frac{h^2}{2m_i}\left(F_{ix}^n + F_{ix}^{n+1}\right) \tag{3.4}$$

Eq. (3.3) and Eq. (3.4) define only the *x* components of the Verlet velocity algorithm. Where the forces, F_{ix}, are derived from the gradient of the potential energy function. Positions and velocities at the starting point of the algorithm, i.e. at time step zero ($n = 0$) are needed to solve the Equations (3.3) and (3.4). This can be done taking into account the physical conditions at the beginning of the system at time zero. In a system with *N* atoms, the number of starting positions and velocities will be 6*N*. For this reason, initial atomic positions can be evaluated as an ideal crystal atomic locations. In order to determine the initial atomic velocities, the Maxwell velocity distribution can be used for the desired temperature of the system [1, 69-71].

The MD algorithm of a physical system computes the positions and velocities (from Eq. (3.3) and (3.4)) for time steps with a selected size, $h = \Delta t$. The basic structure of such an algorithm is given below:

***NVE* Algorithm** [71]

1) Start
2) For $n = 0$, define the initial values of x_i^0 and $v_i^0$and calculate the expression f_{ix}^0.
2) Advance the positions by *h*, using (3.3).
3) Calculate f_{ix}^{n+1} forces using x_i^{n+1} locations.
4) Advance velocities by h, using (3.4).
5) Taking $n \Leftarrow n + 1$ (i.e. increasing *n* by 1) return to step 2.
6) Stop

3.2. Embedded Atom Method

In order to model the physical interactions of metals and alloys, many-body potential functions can be used. The most common potential approach in the concept of many-body interactions is known as the embedded atom method (EAM) [34]. In the EAM approach, the energy of an atom in a crystal is expressed as the sum of the electrostatic repulsion energies and the sum of the embedding energies that define attractive interactions resulting from the electron charge density resulting from neighboring atoms in the atomic coordinates. Thus, the total potential energy of a crystal with *N* atoms can be written as [36]:

$$E_T = \sum_{i=1}^{N} E_i \tag{3.5}$$

$$E_i = \frac{1}{2}\sum_{j\neq i}^{N} \phi(r_{ij}) + F_i(\bar{\rho}_i) \tag{3.6}$$

$$\bar{\rho}_i = \sum_{j\neq i}^{N} \rho(r_{ij}) \tag{3.7}$$

In here, the pairwise interaction function that defines the repulsive interactions is $\phi(r_{ij})$, $\rho(r_{ij})$ is a function of electrostatic charge density at the *i*th coordinates, arising from all neighboring atoms, and $F_i(\bar{\rho}_i)$ is a functional defining the embedding energy. There are different versions of the EAM approach depending on these three functions. Some of them are the Finnis-Sinclair (FS) [73], Johnson [74], Voter-Chen (VC) [75] and Sutton-Chen (SC) approaches.

The force acting on an atom *i* in the EAM approach is derived from the gradient of the potential energy expressions [34].

Various studies have been carried out in order to define the interatomic interactions for different compositions of NiAl alloys. The newest one is the approach developed by PurjaPun and Mishin [46] in 2009, and it can calculate many properties of NiAl alloy in agreement with experimental results.

3.2.1. Embedded atom method by PurjaPun-Mishin

In order to do safely computer simulations in atomic level of the NiAl alloy system, the EAM approach developed by PurjaPun and Mishin [36] and its parameters can be used, as for the other studies [76, 77]:

$$\Phi(r) = \psi\left(\frac{r-r_c}{h}\right)\left[\frac{V_0}{b_2-b_1}\left(\frac{b_2}{z^{b_1}} - \frac{b_1}{z^{b_2}}\right) + \delta\right] \tag{3.8}$$

Where z = r/r_0 and the remaining constants b_1, b_2, V_0, h, and δ are the potential function parameters. These parameters in the potential energy function are obtained to be fitting with the experimental data of the system. If the electron charge density is

$$\rho(r) = \psi\left(\frac{r-r_c}{h}\right)[A_0 z^y e^{-\gamma z}(1 + B_0 e^{-\gamma z}) + C_0] \tag{3.9}$$

Here, the constants A_0, B_0, C_0, r_c, h, y and γ are known as function parameters.

To define NiAl atomic interactions by PurjaPun and Mishin

$$\phi_{\mathrm{NiAl}}(r) = \psi\left(\frac{r-r_c}{h}\right)\left[a_1 e^{-b_1 r}\phi_{\mathrm{NiNi}}\big(c_1(r-r_1)\big) + a_2 e^{-b_2 r}\phi_{\mathrm{AlAl}}(c_2(r-r_2))\right] \tag{3.10}$$

is used [46]. Here, the multiplier function defined by ψ (x) is called the potential cutoff function and it is defined as follows;

$$\psi(x) = \begin{cases} \frac{x^4}{1+x^4}, & x < 0 \\ 0, & x \geq 0 \end{cases} \tag{3.11}$$

This function guarantees that the potential falls off smoothly at the r_c cutting distance. Thus, there are a total of ten fit parameters, a_1, a_2, b_1, b_2, c_1, c_2, r_1, r_2, r_c and h. In order to determine these parameters, the experimental lattice parameter (a_0), formation energy (E_f) and elastic constants (c_{ij}) are used in the B2 phase of the alloy. The formation energy of a NiAl alloy with a Ni_nAl_m composition can be found from the following equation:

$$E_f = \frac{E_0(Ni_nAl_m) - nE_0(N_i) - mE_0(Al)}{n+m} \tag{3.12}$$

Where E_0 describes the cohesive energy of individual elements or alloys [36]. The melting temperatures of the Ni, Al and NiAl alloys determined by using the potential function and the experimental values of them are given in Table 3.1 for comparison with each other [1].

The potential function developed by PurjaPun and Mishin gives very good results in many phases of the NiAl alloy, and the presence of a large number of potential parameters make it difficult to analytically calculate the functions. By preparing the numeric tables of $\Phi(r)$, $\rho(r)$ and $F(\rho)$ functions and using them in a interpolation algorithms provide great advantages when using the functions in some professionally written software, so that such multi-parameter functions can be easily evaluated in simulation studies [1]. For this reason, some simulation researchers produce these tables and present them to usage of the other users on the reliable internet sites. A tabulated version of this potential energy functions can be obtained from the website given in [78]. In this thesis, a tabulated force field form of the PurjaPun and Mishin EAM was used.

Table 3.1 Experimental and calculated melting temperatures for some phases of Ni, Al, and NiAl alloys. Values are in Kelvin units [36].

Phase	Ni	Ni_3Al	NiAl	Al
EAM (Mishin)	1701	1678	1780	1042
Experimental	1728	1645	1911	933
Difference	1.6	1.9	6.8	11.7

3.3. Software's for Molecular Dynamics Simulations

In order to perform the MD simulation study, one of the MD algorithms mentioned above and the analytical forms of the potential energy function suitable for the system to be operated must be coded by using any computer programming language [1]. Fortran, C/C ++, Java, or other programming languages must be well known for this purposes. Furthermore, if high computational speeds are needed, parallel computation techniques must also be known. Fortunately, there are non-commercial and commercial MD simulation packages on the internet resources [29]. Some of these software is given in Table 3.2 [1]. In this thesis, the LAMMPS simulation package [30] given in Table 3.2 are used. Also, as a potential energy functions, PurjaPun and Mishin EAM functions described in the previous section are used. LAMMPS source codes were compiled on the Linux (Ubuntu) operating system and some of the calculations were performed on the TRGRID network [79], which is a national computing network supplied by ULAKBIM in Turkey. The results were evaluated using a personal computer with Intel i7 processor.

Table 3.2. Some of software names and usage [1].

Package Name	Usage Area	License	Access
NAMD+ VMD	Fast, Parallel MD, CUDA	Open source, Academic use	Beckman Institute
LAMMPS	Has potential functions for solid and soft materials	Free, open source. (GNU GPLv2)	Sandia
GROMACS	High Performance MD	Free	gromacs.org
CHARMM	Production of potential energy functions of molecular structure.	Free	charmm.org
BOSS	OPLS	(GNU GPLv2)	Yale University
AMBER	Production of potential energy functions of molecular structure.	Commercial	ambermd.org
ACEMD	MD simulation using CHARMM or AMBER force fields. It can run on NVIDIA GPU using highly optimized CUDA.	Commercial	Acellera Ltd

3.4. LAMMPS Package

The LAMMPS codes started to have been written in the mid-1990s under the leadership of Steve Plimpton as a result of a research and development agreement between Sandia and LLNL laboratories [29]. The main objective of LAMMPS codes is to develop large-scale parallel classical molecular dynamics simulations. Today LAMMPS is offered to scientists as an open-source code with C++ version. In recent years, all developments in molecular dynamics calculations have been tracked and added to this code, thus ensuring that the code remains up-to-date [1]. In a molecular dynamic simulation studies using LAMMPS codes; it is enough to describe the potential energy function, initial atomic positions and simulation parameters in a single input file. Depending on the request, this data can also be supplied using different files. In addition, the user can select which quantities to calculate in the simulations and which result files to generate [1]. Using these codes, it is possible to run the molecular dynamics simulations with millions of particle systems, due to the ability of usage parallel calculations. The common massage passing interface (MPI) libraries for parallel calculations can be used, as well as OpenMP or GPU (CUDA and OpenCL) accelerator options [1].

Especially for simulating the high-level and complex structural system, one can use the ability of LAMMPS which has easily usage of the potential energy functions in the code structure, such as EAM, MEAM, Stillinger-Weber, Tersoff and ReaxFF. These properties make the LAMMPS codes superior to others [1]. There are also utilities such as VMD [68] and OVITO [80] that can be used to analyze LAMMPS simulation results. VMD and OVITO are very useful in visualizing the results, creating animations and performing structural analyzes. Some of the commonly used commands in the input file of the LAMMPS package and their intended use are given in Table 3.3 [1].

Table 3.3. Some commonly used LAMMPS codes and their usage [1, 29].

CODE	USAGE
units	Units in the simulation system.
dimension	Dimensions in the calculation that would be used.
boundary	Determination of the directions to apply the periodic boundary condition
lattice	Assignment of lattice model and lattice constant values
read_data	Define the initial atomic coordinates file
pair_style	Atomic interactions, choice of potential function type
pair_coeff	Identification of potential function parameters and interaction file
group	Definition of a specific atomic group
timestep	Defining the size of time step for integration
velocity	Set up of initial atomic velocities and definition of temperature
compute	Calculation of desired quantities
thermo	Defining the printing frequency and quantity of the results
dump	Option to print atomic coordinates and quantities to file
fix	Define MD parameters
run	Defining the number of integration steps of whole simulation

4. RESULTS AND DISCUSSIONS

This chapter was organized to be composed of three sub-sections as follows: The first section Setup for Model Alloys has been given, which include the constructions of model structures based on polycrystalline concept, by using some computer code packages. Secondly, section Thermodynamic Properties of Models has been given. Also this chapter includes some thermodynamic variations of the model structure, depending on the size of models and the number of grains in the models. As the third and final section, Stress-Strain Behavior of Model NiAl Nanowires has been used as a title, which includes the all of the results obtained from the simulations studies.

4.1. Construction of Polycrystalline Model Alloys

There are many ways to construct the grained structures of the alloys. The easiest and tested way for this purpose is to use Voro++ software library [81]. There is also a code package that uses this library, LATGEN [42]. After installing these code packages on Linux machine the model structures can be setup easily by answering the questions asked by LATGEN code. The main menu window of the LATGEN after the run looks as follow:

```
LatGen version 1.50, compiled on Apr 16 2015.

=============================================
Please select the lattice type of your system:
 1. FCC/Diamond;               |  4. A3B;
 2. BCC;                       |  5. A2B;
 3. HCP/Graphene;              |  6. AB & ABXn;
-------------------------------+-----------------------------------
 7. User defined;              |  8. Multi-layer.
-------------------------------------------------------------------
 9. Polycrystal;               |  0. Exit.
-------------------------------------------------------------------
Your choice [1]:
```

After the choice Polycrystal, entering 1 as an option in main menu, the LATGEN code ask some specific questions more to descript the model structure as follow:

```
lattice type of your system : FCC, BCC, A2B, A3B, etc.
lattice constant of the crystal : a scaler number.
orientation of the lattice : (001), (110) or (111)
type of BCC(001) surface : orientation or B2 structure
the lower and upper bound of the box for x, y or z directions:0 50
periodic boundary conditions in x, y or z directions : 0 0 1
desired number of grains : 4
Create substitutional solid solution :
At the end of the process
the filename of the lammps atomic file :  name.pos
```

If one desire to construct the substitutional alloy model inside the each grain, it can be done by selecting the 'create substitutional solid solution' option and by answering the some more questions about the percentages of the alloying elements and their types. As an example work for a model system having 4 grains and B2 structure prototype produced by using LATGEN code can be seen in Figure 4.1 as a snapshot getting by using the visualization software Ovito.

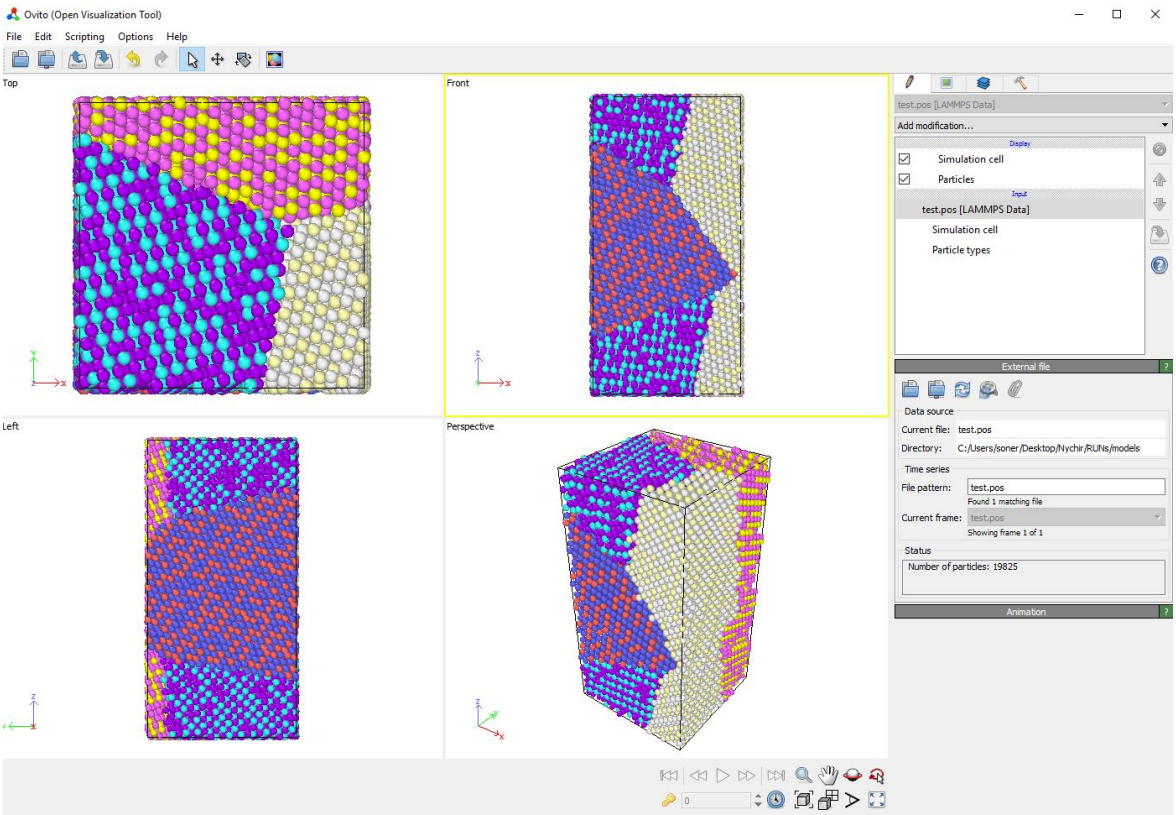

Figure 4.1 A snapshot showing the Ovito software window and a model alloy having 4 grains.

Also some grain properties such as number of vertex, grain volume and number of atoms inside of the grains can be obtained in two files (grain_cell_info and grain_part_info) produced by LATGEN package thanks to voro++ library.

Some of model structures having the cross-section area of 6x6nm^2 and 10nm length produced for simulations in this thesis can be shown in Figure 4.2 as snapshots. Also, the model systems with size of 3x3nm^2 and 10nm length for 3 and 5 grains are given in Figure 4.3. All models produced for tensile loading test here have the same length.

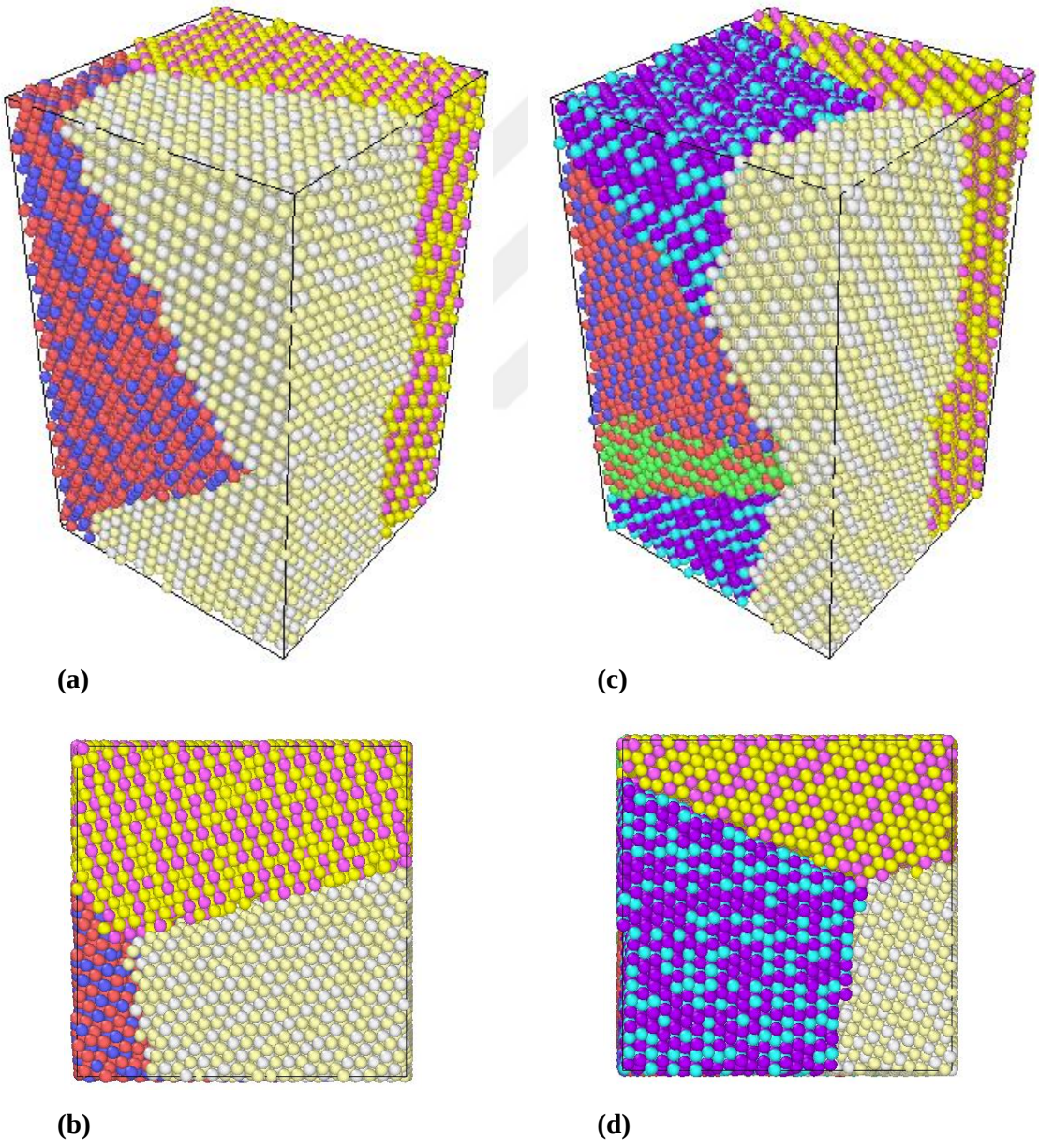

Figure 4.2 Snapshots of the models with 3 grains as **(a)** perspective and **(b)** top views, and 5 grains in **(c)** and **(d)** the same meaning.

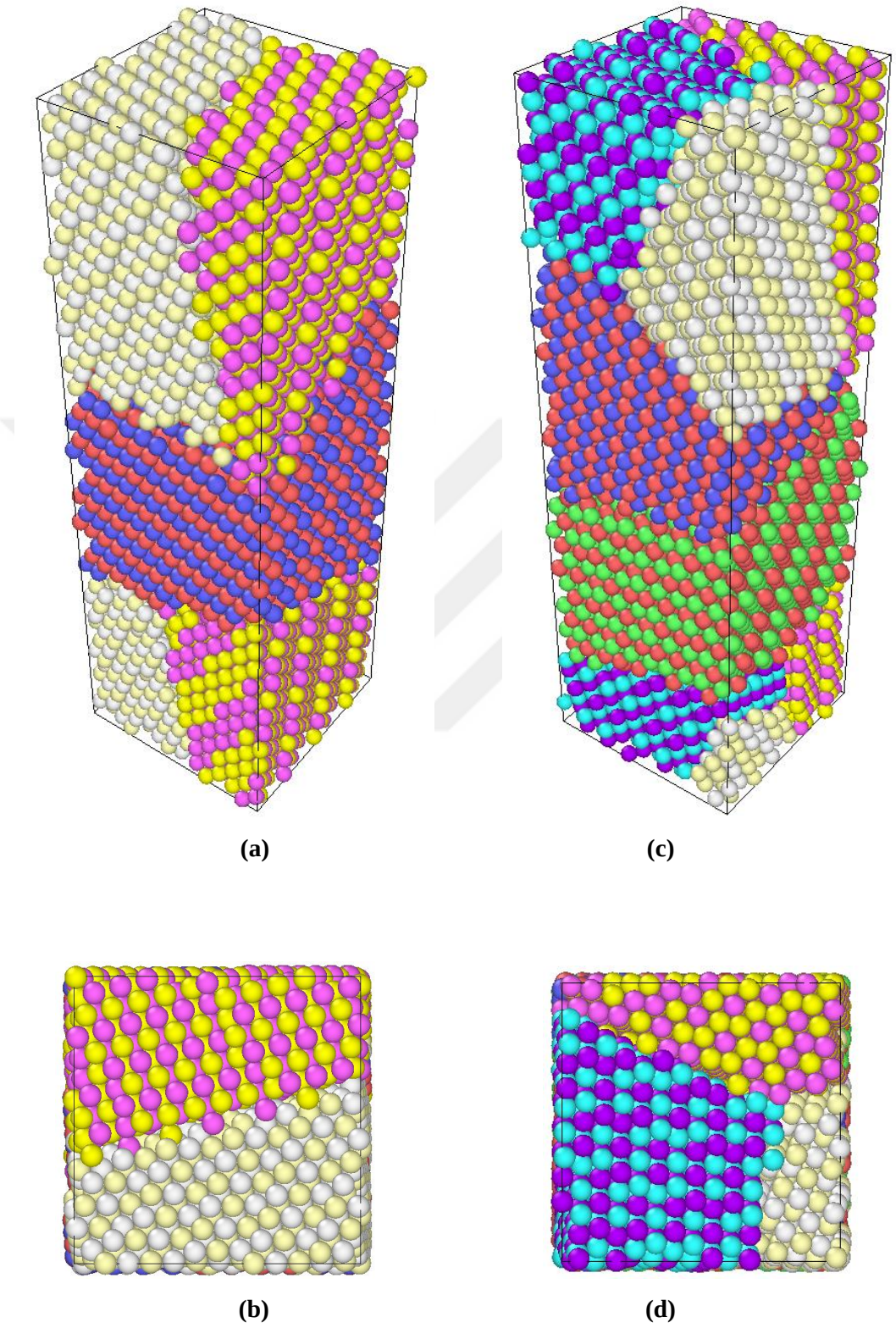

Figure 4.3 Snapshots of models with 3 grains and 3x3nm^2 sized as **(a)** perspective and **(b)** top views, and 5 grains in **(c)** and **(d)** the same meaning.

Also, some properties of the models such as the number of atoms inside the grains and the volume of grains are given in Table 4.1. The total number of atoms inside the model systems are given in Table 4.2. All of the models used in the simulations here have the same length of 10nm. Six different sizes of cross-section area are selected to see the change of stress-strain curve of the models under tensile loading on z direction. When constructing the models with different cross-section area, the shapes of the grains and the crystal orientations inside the grains are kept in the same manner. In this way, it is expected that the only variable governing the change of stress-strain curves is the model size, i.e. the cross-section area. However, it could not possible exactly to keep the shapes constant due to the algorithm producing the grains in voro++ library.

Table 4.1. Some properties of polycrystalline models produced for this thesis.

Model Properties			Model Size (nm^2), regarding the cross-section area.					
			2x2	3x3	4x4	5x5	6x6	7x7
2 Grains	Num. of atoms	G1	1617	3482	5809	8373	11747	15930
		G2	1645	3856	7223	11957	17583	24112
	Volume	G1	19.33	41.62	69.31	100.14	141.29	192.27
		G2	20.66	48.37	90.68	149.85	218.71	297.72
3 Grains	Num. of atoms	G1	1557	3241	5088	6911	9252	12130
		G2	701	1832	3589	6070	9050	12531
		G3	914	2111	4142	7066	10683	14903
	Volume	G1	18.57	38.75	60.84	82.51	110.45	145.07
		G2	8.77	23.05	45.07	76.31	113.08	155.57
		G3	12.64	28.19	54.08	91.16	136.46	189.34
4 Grains	Num. of atoms	G1	1533	3319	5819	5664	12132	15599
		G2	693	1470	2566	5788	6077	8784
		G3	373	725	1358	3289	3646	5262
		G4	314	1032	2193	5084	5836	8517
	Volume	G1	19.06	42.47	73.70	67.65	151.74	193.46
		G2	9.35	19.38	33.24	72.03	77.17	109.95
		G3	5.91	11.10	20.16	42.96	49.94	70.29
		G4	5.65	17.02	32.88	67.35	81.13	116.29
5 Grains	Num. of atoms	G1	1071	2494	4456	6482	8266	10245
		G2	779	1338	1663	2003	2455	3073
		G3	662	1492	2663	4256	6324	8850
		G4	292	715	1614	3043	5090	7479
		G5	332	1016	2214	4024	6493	9465
	Volume	G1	12.79	29.78	53.24	77.36	98.68	122.26
		G2	9.68	17.07	21.53	25.76	31.32	39.18
		G3	8.22	18.84	33.68	53.96	80.22	112.08
		G4	4.22	9.91	21.45	39.61	65.29	94.92
		G5	5.07	14.37	30.08	53.28	84.46	121.53

Table 4.2. The total number of atoms inside the model systems.

Model	Model Size (nm^2), regarding the cross-section area.					
	2x2	3x3	4x4	5x5	6x6	7x7
2 Grains	3262	7338	13032	20330	29330	40042
3 Grains	3172	7184	12819	20047	28985	39564
4 Grains	2913	6546	11936	19825	27691	38162
5 Grains	3136	7055	12610	19808	28628	39112

In Figure 4.4, it can be shown the positions of the grain boundaries settled in the tensile loading direction in some model systems. In this figure, partially periodicity are shown on z direction. Also, to perform tensile tests, approximately 10% of the geometrically lower parts of these models and 10% of the upper parts are fixed as the solid parts which they play a role as grip section in real tensile experiments. MD calculations are made over the remaining 80% of the models which can be stretchable dynamically.

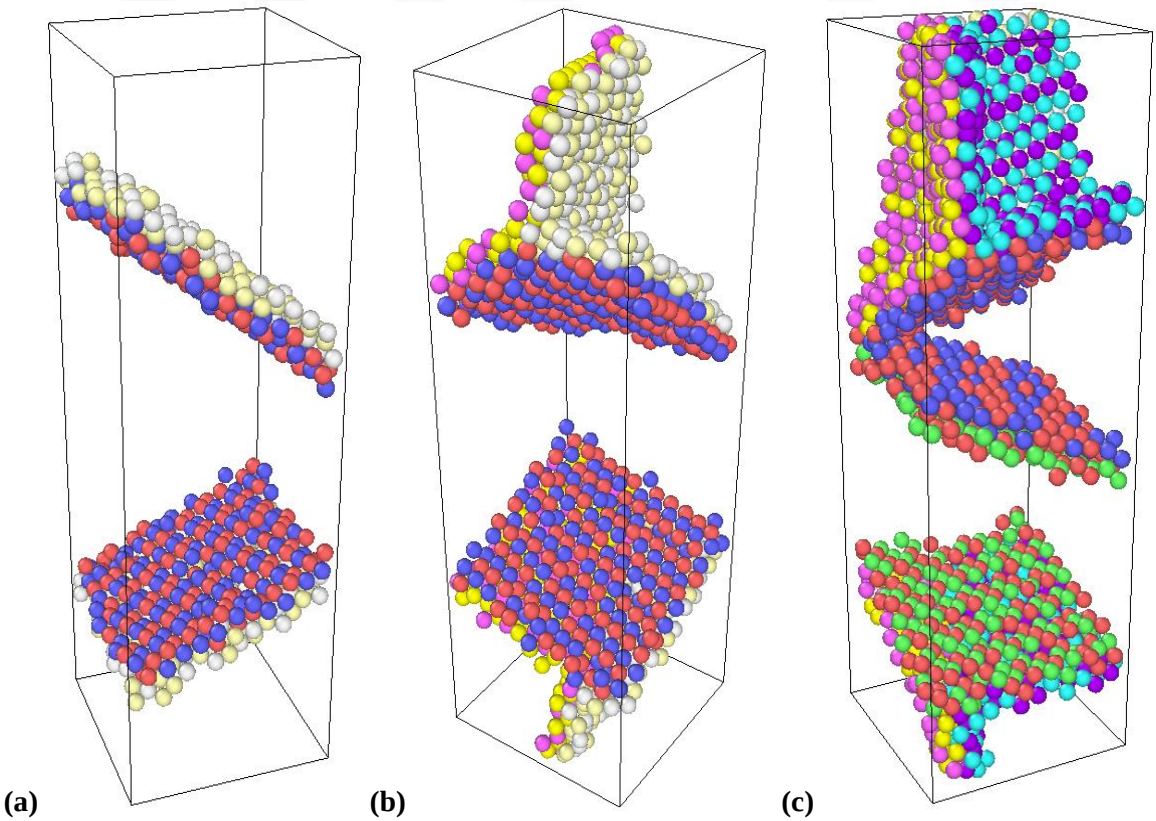

Figure 4.4. Grain boundary profiles of 3x3nm^2 sized models, and for **(a)** G2, **(b)** G3, and **(c)** G5 grains.

After the model constructions, all of the models are relaxed thermodynamically in order to get their equilibrated structures before the tensile loading. The relaxation behaviors and some thermodynamic properties of the models are given in the next section.

4.2. Thermodynamic Properties of Models

The model systems are relaxed in a dynamic process in order to get their minimum energy structure because it is impossible to setup like that, when the model systems are first constructed with some defective structures as grains. In this dynamic process, it is desired to determine the relaxation behaviors of the models by observing the cohesive energy, volume, temperature, pressure and three axis lengths of the systems. Here, the obtained data are given only for the model G2 with 2x2nm^2 sized to maintain the clarity.

Figure 4.5 shows the cohesive energy change of the G2 2x2nm^2 sized model in the run for relaxation process of totally 20000 MD time steps each of 2fs. Also, initial temperature of the system is set to 300K and Nose-Hoover thermostat procedure applied on the system to maintain the temperature stability. From Figure 4.5, it has been observed that the energy of the model system is almost relaxed at the end of the thermalization process, although excessive fluctuations in the energy are observed in the first part of the run. Relaxed cohesive energy is -4.12eV. There are similar changes in the temperature of the system can be shown in Figure 4.6. The main differences between these two quantities (energy and temperature) is the frequency of the fluctuations. The frequency for temperature oscillations is higher than that of the cohesive energy. This result can be concluded as the atomic movements in the system is high at the beginning of the relaxation process due to the disordering of the grain boundaries. At the end of the relaxation process the average temperature of the system is found to be 300.4K.

Volume and pressure changes of the model system in relaxation process are given in Figure 4.7 and Figure 4.8, respectively. Also, the axial length changes for the same model can be shown in Figure 4.9. If volume, pressure and the Lz changes are examined comparatively, it is easy to say that almost similar changes occur. Hence, these changes are caused by systematically length oscillations especially in the *z* direction, but non-systematic changes is observed in *x* and *y* directions, which is most probably due to the periodic boundary conditions that applied only on *z* direction. After the equilibration phase, the average length in *z* direction is found to be 9.685nm. However, this value was set to 10.0nm during the construction of model.

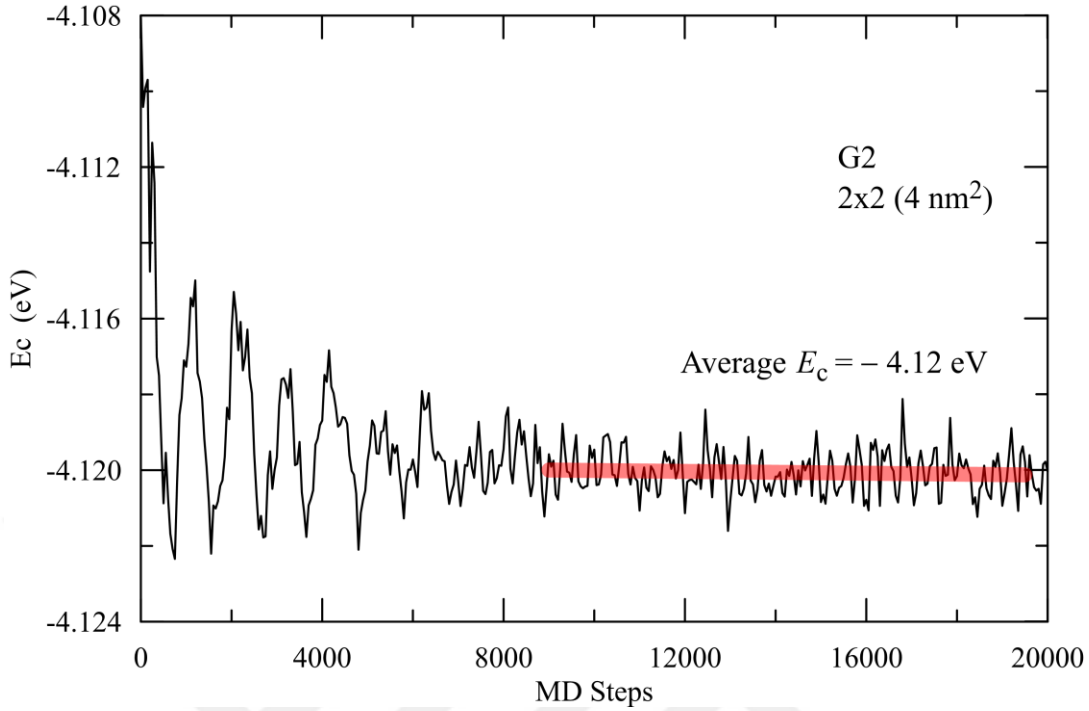

Figure 4.5. Cohesive energy change of the G2 model with 2x2nm^2 in thermalization process.

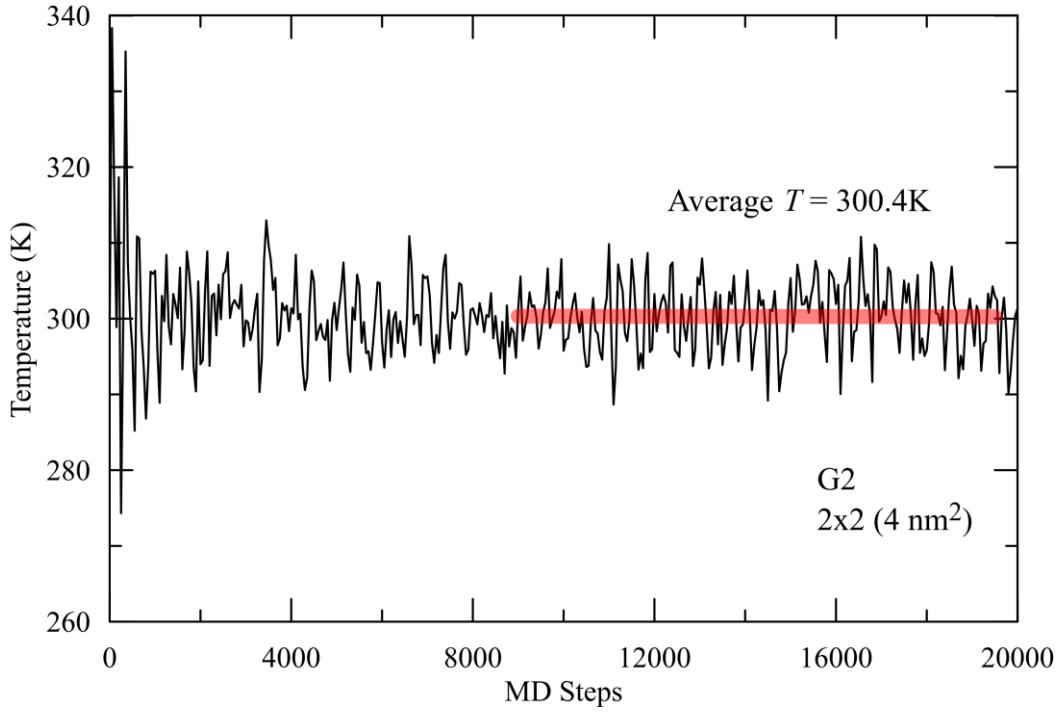

Figure 4.6. Temperature change of the G2 model system with 2x2nm^2 in thermalization process.

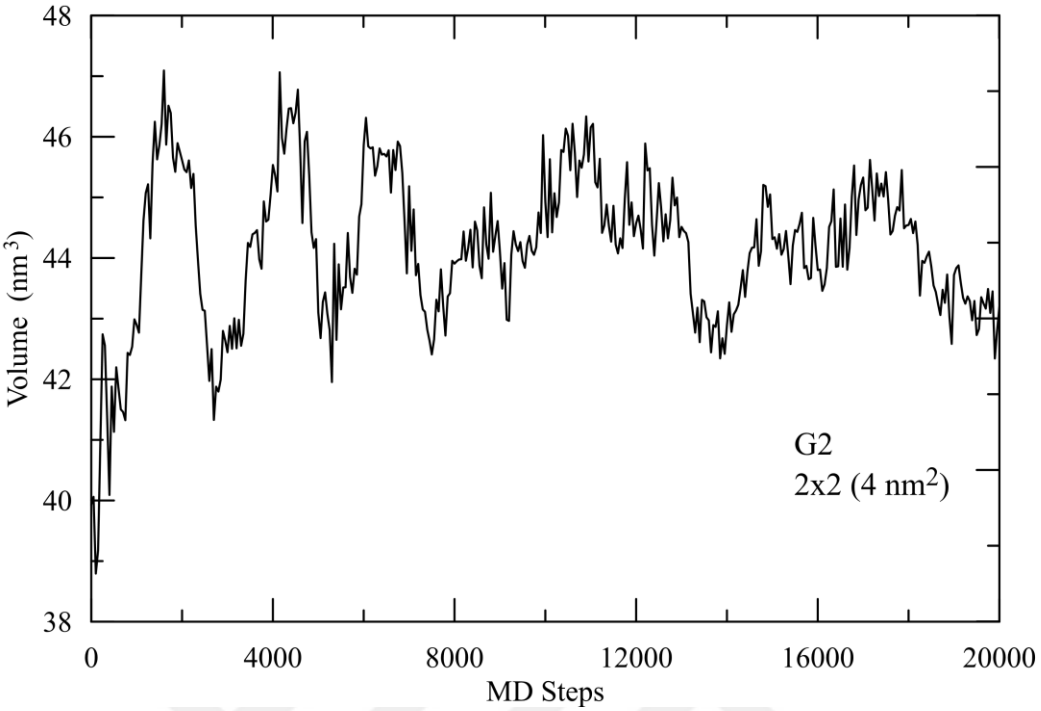

Figure 4.7. Volume change of the G2 model system with 2x2nm^2 during thermalization process.

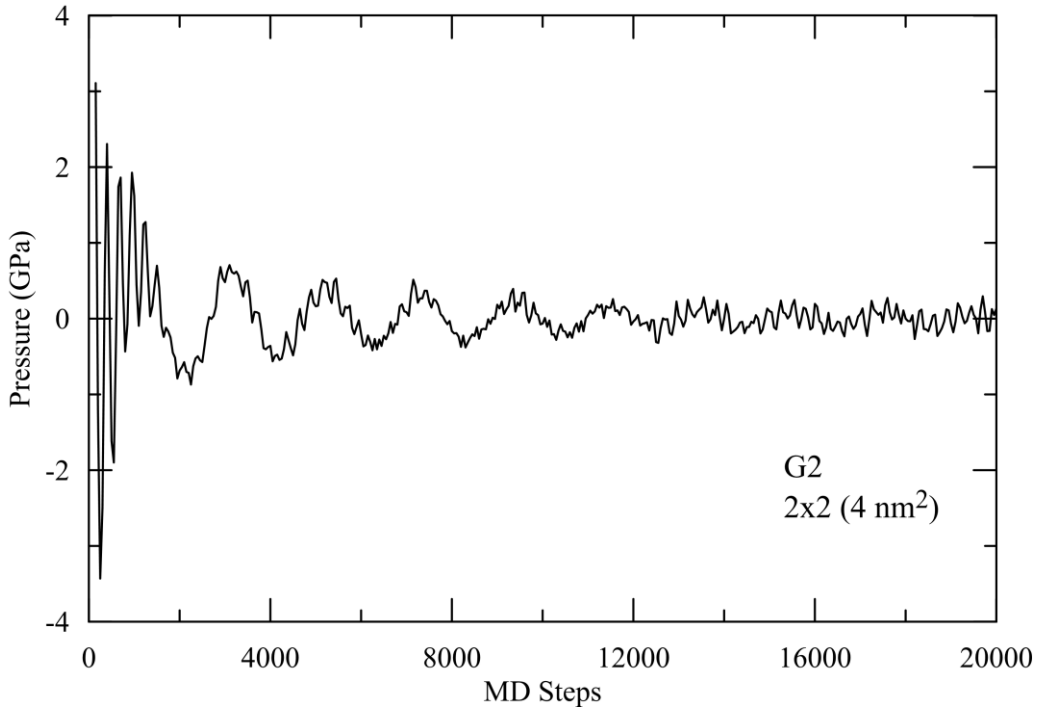

Figure 4.8. Pressure change of the G2 model system with 2x2nm^2 during thermalization process.

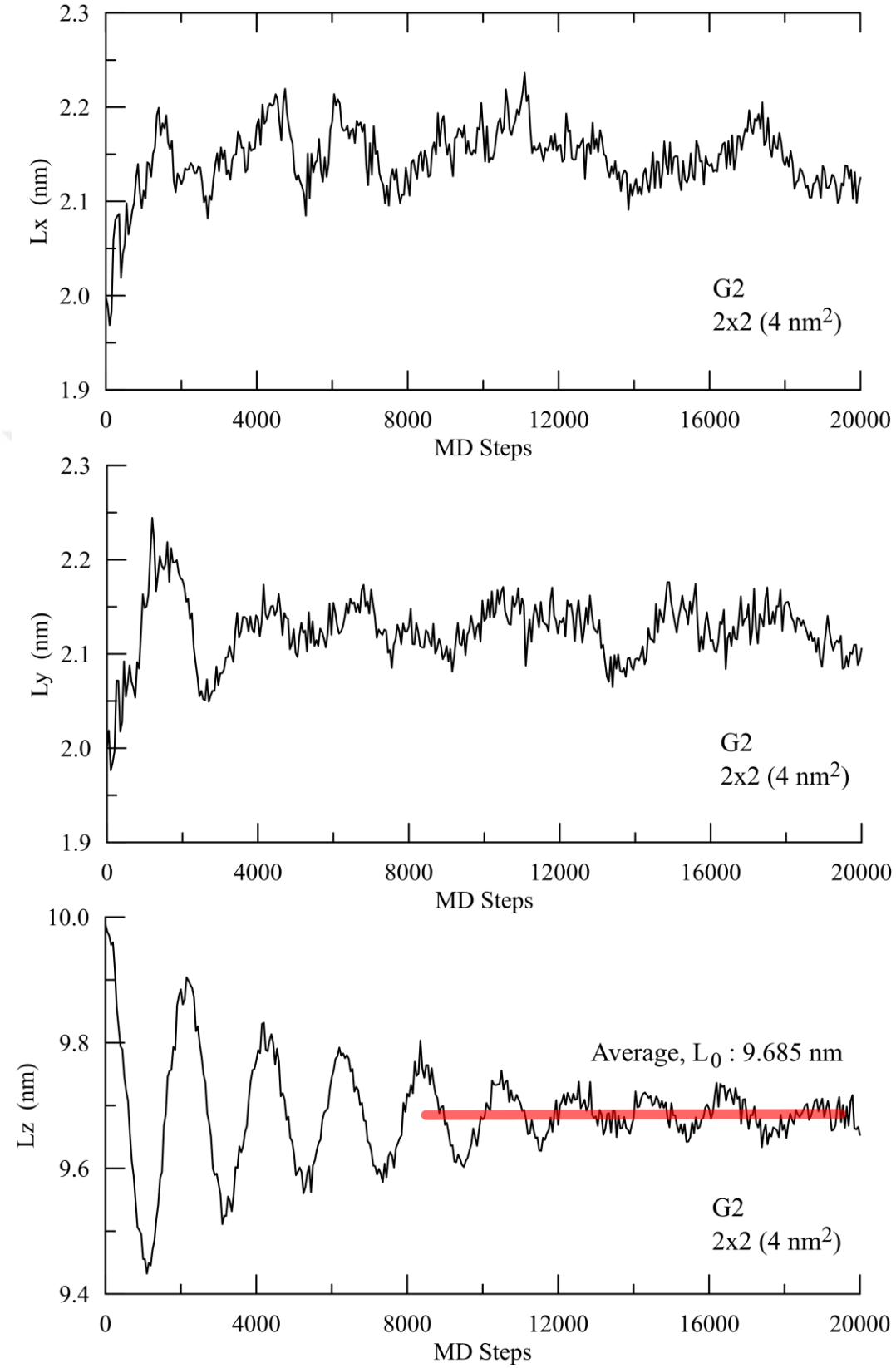

Figure 4.9. Axial length changes of the G2 model system with 2x2nm^2 during thermalization process.

4.3. Stress-Strain Behavior of Model NiAl Nanowires

Before examining the stress-strain behavior of the models; the time behavior of some quantities such as cohesive energy, volume and internal stress were observed while tensile loading for the sample sized 7x7nm^2 and containing 2 grains. The change in cohesive energy over time is shown in Figure 4.10. There is a proportional change in the first 20000 MD steps region before the plastic deformation begins. The energy in this region has increased by about 0.02eV. It is known that this region is the elastic zone. Then, with the deformation in the structure, the rate of energy exchange slows down. A plateau with an energy of about 4.30eV up to 200,000 steps, and then increases again to an order of magnitude of 4.285 eV.

In Figure 4.11, the change in volume for the 2 grained model with 7x7nm^2 size is shown upon tensile loading. Here, too, there is a steady increase in model volume as increasing the stress, mainly by 200,000 steps, but then a rapid increase can be seen in volume. In this process the volume has doubled. The volume of the first model has 490nm^3, but then it reached about 1000nm^3.

Another quantity that its change was monitored over time is the internal stress calculated on direction *z* and is given in Figure 4.12. The change in stress over time up to 20,000 is also given in the same figure as for clarity.

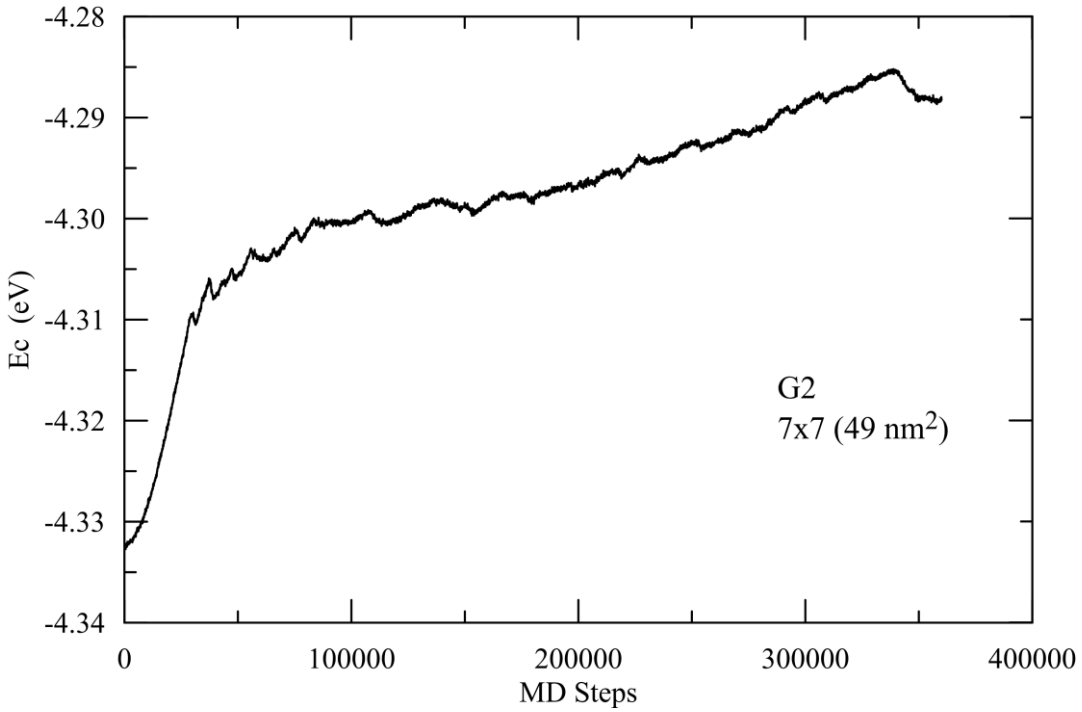

Figure 4.10. Change of cohesive energy under tensile loading test of 7x7nm^2 sized model with 2 grains.

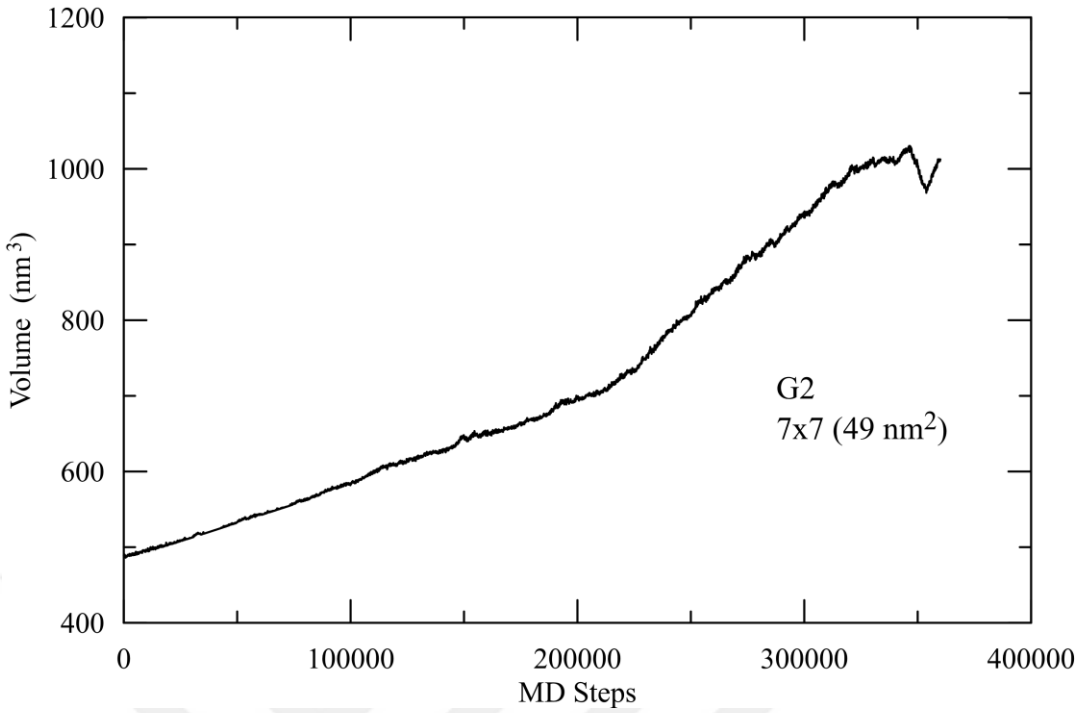

Figure 4.11. Change of volume of the 7x7nm^2 sized model with 2 grains under tensile loading test.

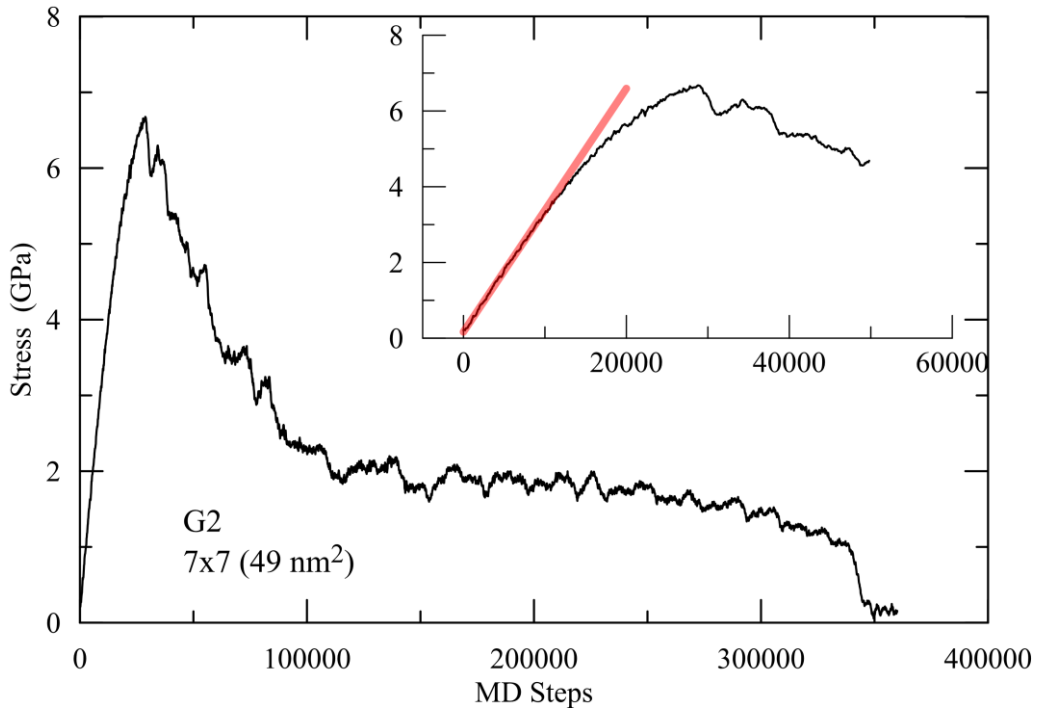

Figure 4.12. Change of internal stress of the 7x7nm^2 sized model with 2 grains during tensile loading.

Once the quantities have been monitored with respect to time relations, stress-strain curves of all models have been obtained. Since it is not possible to give all data of studies here, only some selected results of models are given here. The stress-strain curve of the 2x2 and 2 grained models, the simplest model, are shown in Figure 4.13. The linear change on the curve up to the first 0.01 strain value has been used in the calculation of the Young's modulus, as made for each model.

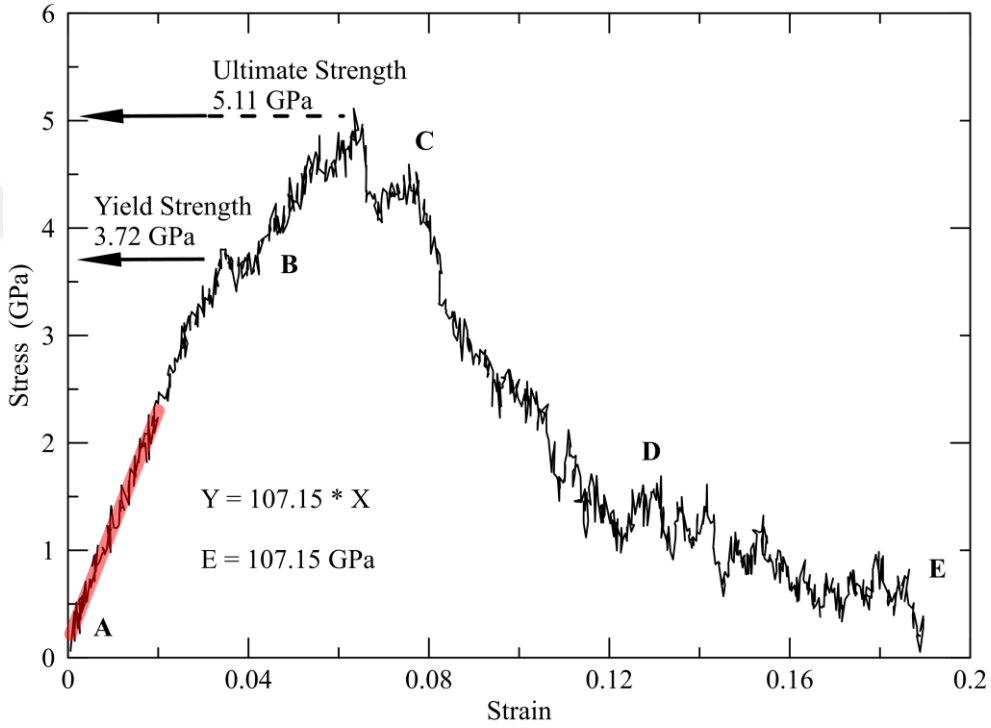

Figure 4.13. Stress-strain curve of 2x2nm^2 sized model with 2 grains.

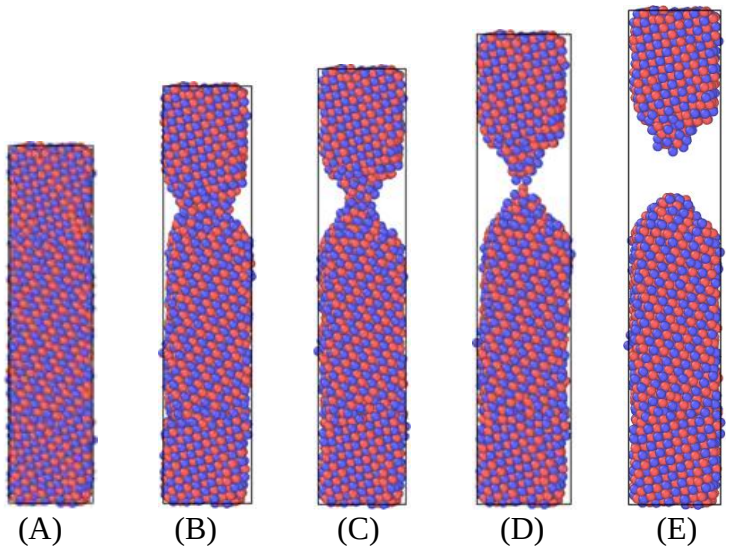

Figure 4.14. Structural change of 2x2nm^2 sized model with 2 grains during tensile loading.

Also, structural changes during tensile loading is given in Figure 4.14. Points marked A, B, C on the curve in Figure 4.13 represent the same points as those defined in Figure 4.14. So one can follow the structural changes during tensile loading. At the same time, once the stress-strain curve was determined, then the yield strength and ultimate tensile strength of the material can be obtained easily, as can be seen in Figure 4.13. The yield strength of the material is defined as the point at which the linear zone ends and the plastic deformation begins as increasing the strain. Also, ultimate tensile strength of the material is defined as the maximum peak value before the necking is seen. According to these definition, for the model with $2x2nm^2$ size and 2 grains, it has been determined that the yield strength and ultimate tensile strength are 3.72GPa and 5.11GPa, respectively. Also, in Figure 4.13 it has been shown that the smallest model is broken at a strain value of approximately 0.19. Before the fracture, at point D the model can stand thanks to only a few atoms attractions. At that point and the crack region of the material the structure become an amorphous state. At the same time, this crack occurrence begins in the upper grain boundary. This observation is consistent with the results of other studies. The grain boundaries are known as the weak points of the material from the energy point of view.

Similar results were obtained for the other models and the results for 4x4 and 6x6 sized model with 2 grains are given in from Figure 4.15 to Figure 4.18. The stress-strain curve of model with size of $4x4nm^2$ are shown in Figure 4.15. The main difference from $2x2nm^2$ sized model is the fracture point. While the thinner model has lower fracture value of 0.19 in strain, $4x4nm^2$ sized model has approximately 0.3, in Figure 4.15, and $6x6nm^2$ sized model has about 0.6 as can be seen in Figure 4.17. In Figure 4.16 and 4.18, the grain boundary motions can be seen clearly upon tensile loading increase over 0.04, sliding over each other. Also, it has been found that the Young's modulus increases as the thickness of model increases.

All of Young's modulus determined here are given in Table 4.3. It has been observed that as the grain number increases, the value of Young's modulus decreases, but increases as the size of the model increases. Also these changes are given in Figure 4.19 and Figure 4.20.

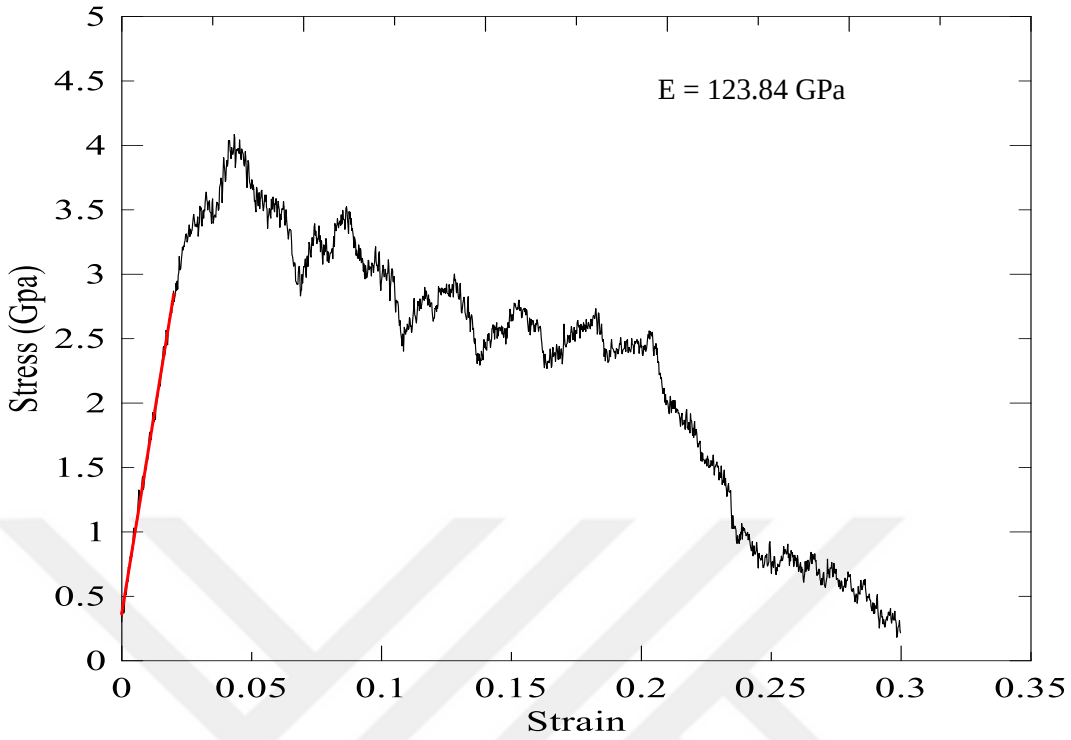

Figure 4.15. Stress-strain curve of 4x4nm^2 sized model with 2 grains.

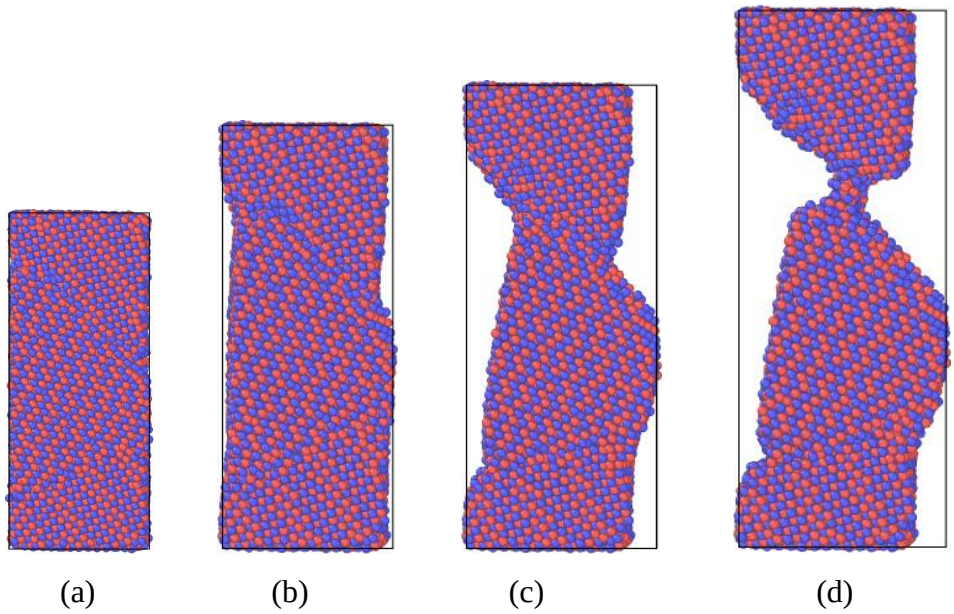

Figure 4.16. Structural change of 4x4nm^2 sized model with 2 grains during tensile loading.

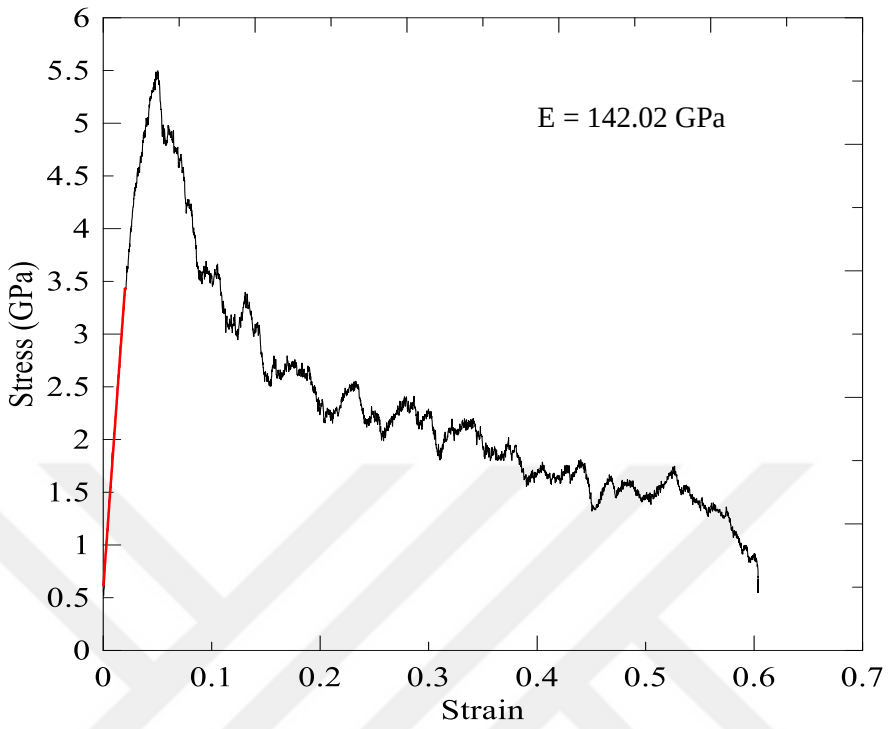

Figure 4.17. Stress-strain curve of 6x6nm^2 sized model with 2 grains.

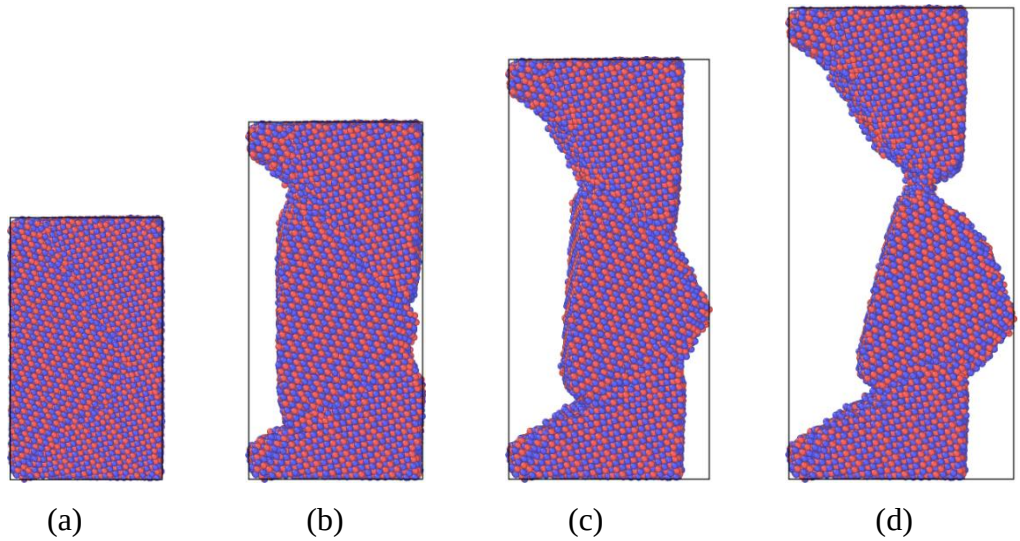

Figure 4.18. Structural change of 6x6nm^2 sized model with 2 grains during tensile loading.

Table 4.3. Young's modulus of NiAl nanowire models.

Model	Size (nm^2)					
	2x2	3x3	4x4	5x5	6x6	7x7
2 Grains	107.15	116.77	123.84	125.12	142.02	156.64
3 Grains	113.10	116.80	127.84	128.57	146.21	149.93
4 Grains	77.45	102.34	108.57	128.40	124.57	121.93
5 Grains	85.28	97.51	107.15	106.91	128.19	127.42

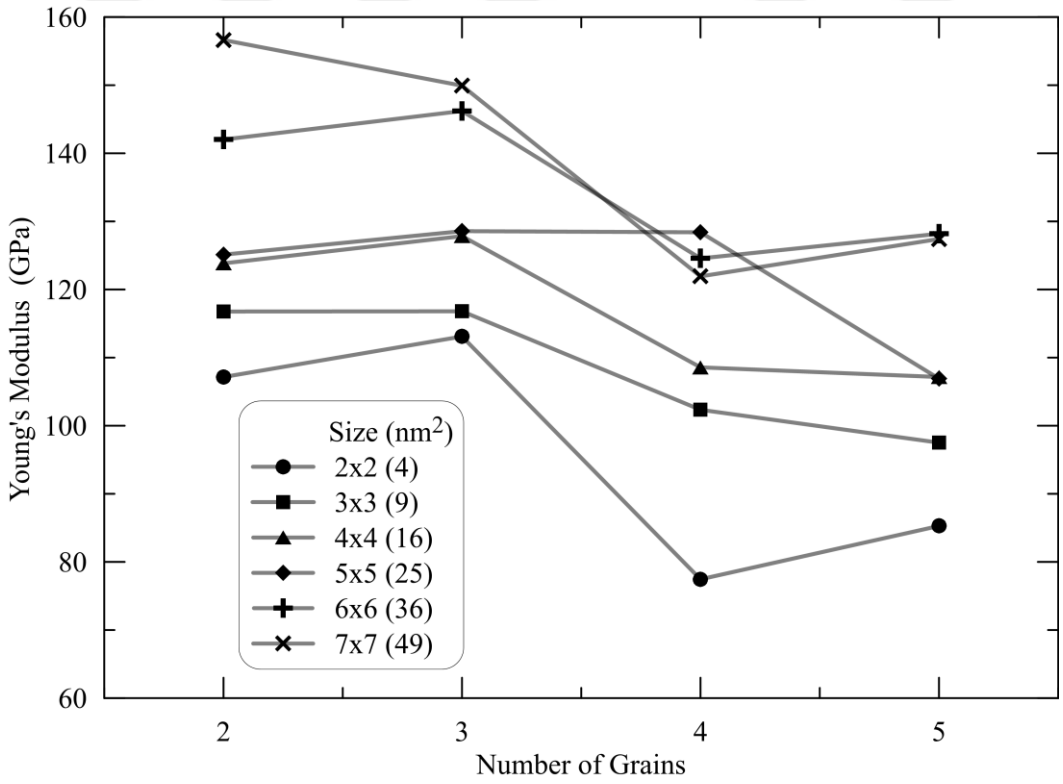

Figure 4.19. Changes of Young's modulus with respect to the number of grains.

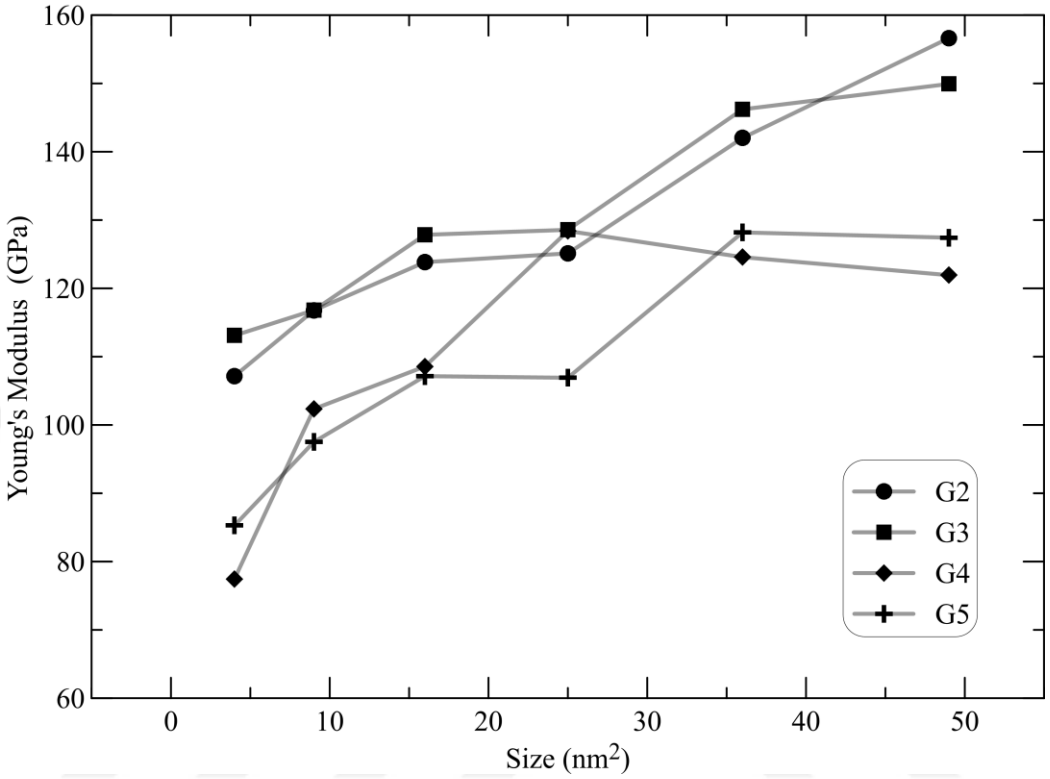

Figure 4.20. Changes of Young's modulus with respect to the size of the models.

Molecular dynamics simulation was used to study the deformation of polycrystalline NiAl nanowires subjected to uniaxial tensile stress at 6 different thicknesses and 4 different number of grains with constant stress rate and temperature, employing embedded atom method (EAM).

We investigated mechanical properties of the nanowires by calculating the stress-strain response of the nanowires and as a result the change of Young's modulus was achieved. We have realized the effect of different grain number on the Young's modulus, when the grain number increased the Young's modulus decreases but increase as the size of model increases. It was also found the effect of the thickness of the models on the Young's modulus, as the thickness of models increases the Young' modulus increase.

There are too many problems to be solved in this field in the future. In this thesis, it has been aimed to show that these problems can be solved by using the molecular dynamics simulations. Detailed calculations have been left to work in the future.

REFERENCES

[1] **Kuşça H.,** 2015, Investigation of Mechanical Properties of NiAl Nanowires by means of Molecular Dynamics Simulations, MSc. Thesis, Fırat University, Graduate School of Natural and Applied Sciences, Elazığ, in Turkish.

[2] **M.C. Roco**. 2001. A Frontier for Engineering, Mech. Eng. 123, January, 52–55.

[3] **Golovnev, I.F., Golovneva, E.I., Fomin, V.M.**, 2006, The influence of a nanocrystal size on the results of molecular-dynamics modeling, Comp. Matter. Sci., 36, 176-179

[4] **Niu J.J., Zhang J.Y., Liu G., Zhang P., Lei S.Y., Zhang G.J., Sun J.**, 2012. Size- dependent deformation mechanisms and strain-rate sensitivity in nanostructured Cu/X (X = Cr, Zr) multilayer films, Acta Materialia, **60**, 3677-3689.

[5] **Wolf, E.L**., 2004, Nanophsics and Nanotechnology, WILEY-VCH Verlag GmbH &Co. KGaA, Weinheim

[6] **Smith, W.F**., 1996, *Principles of Materials Science and Engineering*, McGraw-Hill Inc., New York, USA.

[7] **Savaşkan, T.,** 2004, *Malzeme Bilgisi ve Muayenesi*, Akademi Ltd. Şti. Yayınları, No:15, Trabzon

[8] **Nouailhat, A.,** 2008. *An Introduction to Nanoscience and Nanotechnology*, ISTE Ltd and John Wiley & Sons, Inc. Britain and the United States

[9] **Ramesh, K.T.,** 2009. *Nanomaterials Mechanics and Mechanisms*, The Johns Hopkins University Baltimore, USA.

[10] **Deng, X., Joseph, V.R., Mai w., Wang Z.L., and Jeff Wu C. F**., 2009, Statistical approach to quantifying the elastic deformation of nanomaterials, Pnas , 29**,** 11845–11850.

[11] **Zhu, Y., Xu, F., Qin,Q., Fung, W. Y., and Lu, W.**, 2009, Mechanical Properties of Vapor-Liquid-Solid Synthesized Silicon Nanowires, Nanoletters, 11, 3934-3939.

[12] **Wood, E.L., Avant, T., Kim, G.S., Lee, S.K., Burchman, Z., Hughes, J.M., Sansoz, F**., 2014 , Size effects in bimetallic nickel–gold nanowires: Insight from atomic force microscopy nanoindentation, Acta Materialia, 66, 32–43.

[13] **Kobler, A., Beuth, T., Klöffel,T., Prang,R., Moosmann,M., Scherer, T., Walheim,S., Hahn, H., Kübel, C., Meyer, B., Schimme, T. and Bitzek, B**., Nanotwinned silver nanowires: Structure and mechanical properties, Acta Materialia, 92 , 299–308.

[14] **Park, H.S. and Klein, P.A.,** Surface stress effects on the resonant properties of metal nanowires: The importance of finite deformation kinematics and the impact of the residual surface stress, Journal of the Mechanics and Physics of Solids,56 , 3144–3166

[15] **Xu, F., Qin, Q.,Mishra, A., Gu, Y., and Zhu, Y.,** Mechanical Properties of ZnO Nanowires Under Different Loading Modes, Nano Res , 3, 271–280.

[16] **Li, H. and Sun, F**., 2012, Recent Advances in Mechanical Properties of Nanowires,Intech, http://dx.doi.org/10.5772/ 52592

[17] **Bruus, H.,** 2004, Introduction to nanotechnology, MIC – Department of Micro and Nanotechnology Technical University of Denmark, Denmark.

[18] **Gogotsi, Y.,** 2006, *Nanomaterials handbook* , Taylor & Francis Group, London New York.

[19] **McDowell, M.T., Leach, A. M., and Gall, K.,** 2008, Bending and tensile deformation of metallic nanowires, Modelling Simul. Mater. Sci. Eng., 16**,** 045003 (13pp)

[20] **Sansoz, F. and Deng, C.,** 2012, Size-Dependent Plasticity in Twinned Metal Nanowires, ICF12, Ottawa 2009.

[21] **Bhatt, J. C., and Kholiya, K.,** 2014, Effect of size on the elastic and thermodynamic properties of nanomaterials, Indian Journal of Pure & Applied Physics, 52, 604-608.

[22] **Kunz, A., Pathak, S., and Greer, J. R.,** 2011, Size effects in Al nanopillars: Single crystalline vs. bicrystalline, Acta Materialia, 59, 4416–4424.

[23] **Tim Wübben, DFG.,** 2013, Nanomaterials, WILEY-VCH Verlag GmbH & Co. KGaA, Weinheim

[24] **Liu, Wei-Ting, Hsiao, Chun-I., Hsu, Wen-Dung.,** 2014, Role of surface on the size-dependent mechanical properties of coppernano-wire under tensile load: A molecular dynamics simulation, Applied Surface Science, 289**,** 47– 52.

[25] **Zhu, T., and Gao, H.**, 2012, Plastic deformation mechanism in nanotwinned metals: An insight from molecular dynamics and mechanistic modeling, Scripta Materialia, 66, 843–848

[26] **Li, Xian-Fang, Zhang, H., Lee, K. Y.,** 2014, Dependence of Young's modulus of nanowires on surface effect, International Journal of Mechanical Sciences, 81,120–125

[27] **Haile, J.M.,** 1992. Molecular Dynamics Simulation, Elementary Methods, John Wiley & Sons, Inc., Canada.

[28] **Mishin, Y., Mehl, M. J., Papaconstantopoulos, D. A., Voter, A. F., Kress, J. D.,** 2001. Structural stability and lattice defects in copper: Ab initio, tight-binding, and embedded-atom calculations, Physical Review B, **63**, 224106.

[29] https://en.wikipedia.org/wiki/List_of_software_for_molecular_mechanics_modeling, 28 Haziran, 2016.

[30] http://lammps.sandia.gov/: 28 Haziran, 2015.

[31] http://www.gromacs.org/: 28 Haziran, 2015.

[32] http://imd.itap.physik.uni-stuttgart.de/: 28 Haziran, 2015.

[33] http://www.ks.uiuc.edu/Research/namd/: 28 Haziran, 2015.

[34] **Daw, S.M., Baskes, M.I.,** 1984, Embedded-Atom Method: Derivation and Application to Impurities, Surfaces, and Other Defects in Metals, Physical Review B, 29, 6443- 6453.

[35] **Mishin, Y., Mehl, M. J**., Papaconstantopoulos, D. A., Voter, A. F. and Kress, J. D., 2001, Structural stability and lattice defects in copper: *Ab initio*, tight-binding, and embedded-atom calculations, Physical Rev. B, 63, 224106.

[36] **PurjaPan, G.P., and Mishin, Y.**, 2009, Development of an interatomic potential for the Ni-Al system, Philosophical Magazine, 34-36, 3245–3267

[37] **Yang, Z., Lu, Z., Zhao, Y.P**., 2009, Atomistic simulation on size-dependent yield strength and defects evolution of metal nanowires, Computational Materials Science, 46, 142-150.

[38] **Baskes, M.I**., 1992, Modified embedded-atom potentials for cubic materials and impurities, Phys. Rev. B 46, 2727.

[39] **Cagin T., Che, J., Qi, Y., Zhou, Y., Demiralp, E., Gao, G., and Goddard III, W. A.,** 1999, Computational Materials Chemistry at the Nanoscale, Journal of Nanoparticle Research, 1, 51–69.

[40] **Park, H. S., Gall, K, Zimmerman, J.A.**, 2006, Deformation of FCC nanowires by twinning and slip, Journal of the Mechanics and Physics of Solids, 54, 1862-1881.

[41] **Huang, D., Zhang, Q., Qiao, P.,** 2011. Molecular dynamics evaluation of strain rate and size effects on mechanical properties of FCC nickel nanowires, Computational Materials Science, 50, 903-910.

[42] https://code.google.com/p/latgen/: 5 Temmuz 2016.

[43] **E.J. Pavlina, C.J. Van Tyne**, 2008. Correlation of Yield Strength and Tensile Strength with Hardness for Steels, Journal of Materials Engineering and Performance, 17(6), 888-893.

[44] **F. Milstein**, 1980. Theoretical elastic behaviour of crystals at large strains. J Mater Sci., 15, 1071–1084.

[45] **P.R.Cantwell et al**, 2014. Grain boundary complexions. Acta Materialia, 62, 1–48.

[46] **R.D. Doherty, D.A. Hughes, F.J. Humphreys, J.J. Jonas, D. Juul Jenson**, et al. 1997. Current Issues In Recrystallisation: A Review, Materials Science and Engineering A, 238 (2): 219–274.

[47] **A.P. Sutton, R.W. Balluffi**, 1987. Overview no. 61: On geometric criteria for low interfacial energy, Acta Metallurgica, 35 (9): 2177–2201.

[48] **Begau, C.,** Characterization of crystal defects during molecular dynamics simulations of mechanical deformation, thesis of Doctor, Faculty of Mechanical Engineering the Ruhr University Bochum, Bochum (Germany) 2012.

[49] **R. Philips,** *Crystals, Defects and Microstructures*. Cambridge University Press, 2001.

[50] **D. Hull and D. Bacon,** *Introduction to dislocations*. Butterworth Heinemann, 4 ed., 2001

[51] **J. Hirth and J. Lothe**, *Theory of dislocations*. Krieger Pub. Co., 2 ed., 1982.

[52] **Nasher, S.H.,** INTRODUCTION /*LEC.NO.(1)/MATERIAL PROPERTIES http://uotechnology.edu.iq/ appsciences/filesPDF/physics/lectures/2c/5-MATERIAL%20PROPERTIES3.pdf* , 29 Nov. 2016.

[53] **Alavi A., Mirabbaszadeh K., Nayebi P., Zaminpayma E.**, 2010. Molecular dynamics simulation of mechanical properties of Ni-Al nanowires, Computational Materials Science, **50**, 10-14

[54] **T.G. Nieh, J. Wadsworth**, 1991. Hall–Petch relation in nanocrystalline Solids, Scr. Metall. Mater, 25:955.

[55] **R.O. Scattergood, CC.A. Koch**, 1992. A modified-model for Hall–Petch behavior in nanocrystalline materials. Scr Metall Mater., 27:1195

[56] **J. Schiotz, K.A. Jacobsen**, 2003. Maximum strength of nanocrystalline copper, Science, 301:1357.

[57] **RA. Masamura, PM. Hazzledine, PK. Liaw, EJ. Lavernia**, 1998. Yield stress of fine grained materials. Acta Metall., 13:4527.

[58] **H. Conrad, J. Narayan**, 2000. On the grain size softening in nanocrystalline materials. Scr Mater., 42:1025.

[59] **H. Van Swygenhoven, M. Spaczer, A. Caro**, 1999. Microscopic description of plasticity in computer generated metallic nanophase samples: a comparison between Cu and Ni. Acta Mater., 47:3117.

[60] **V. Yamakov, D. Wolf, SR. Phillpot, AK. Mukherjee, H. Gleiter**, 2004. Deformation-mechanism map for nanocrystalline metals by molecular dynamics simulation. Nat Mater., 3:43.

[61] **K. Lu, ML. Sui**, 1993. An explanation of the Hall–Petch law in micro and nanocrystalline materials. Scr Mater., 28:1465.

[62] **PP. Chattopadhyay, SK. Pabi, I. Manna**, 2000. On the inverse Hall–Petch relationship in nanocrystalline materials. Z Metall., 91:1049.

[63] **E.O. Hall**, 1951. The deformation and aging of mild steel. Proc Phys Soc London B, 64:747

[64] **N.J. Petch**, 1953. The cleavage strength of polycrystals. J. Iron Steel Inst., 25:174.

[65] **J. Eckert, J.C. Holzer, C.E. Krill, W.L. Johnson**, 1992. Structural and thermodynamic properties of nanocrystalline FCC metals prepared by mechanical attrition. J Mater Res., 7:1751.

[66] **Meyers MA, Mishra A, Benson DJ** (2006) Mechanical properties of nanocrystalline materials. Progr Mater Sci 51(4):427–556

[67] **Lu K, Lu L, Suresh S**, (2009) Strengthening materials by engineering coherent internal boundaries at the nanoscale. Science 324(5925):349–352

[68] **G.J. Ting, D.X. Hao, L. Gusong.** 2004. Continuous Dynamic Recrystallization of Extruded Nial Polycrystals During Superplastic Deformation Process, 24th International Congress Of The Aeronautical Sciences, 29 August – 3 Sept. 2004, Yokohama, Japan.

[69] **Haile, J. M.,** 1992, *Molecular Dynamics Simulation, Elementary Methods*, John Wiley & Sons, Inc., Kanada.

[70] **Rapaport, D.C.**, 2004, *The Art of Molecular Dynamics Simulation*, Cambridge University Press.

[71] **Özgen, S.**, 1997, Sayısal hesaplama yöntemlerinin şekil hatırlamalı alaşımlarda difüzyonsuz dönüşümlere uygulanması, Doktora Tezi, Fırat Üniversitesi, Fen Bilimleri Enstitüsü, Elazığ.

[72] **Sun, D. Y., and Gong, X.G.,** 2002, A new constant-pressure molecular dynamics method for finite systems, J. Phys. Condens Matter, 14, L487-L493.

[73] **Finnis, M.W. and Sinclair, J.E.**, 1984, A Simple empirical N-body potential for transition metals, Philos. Mag., A, 50(1), 45-55.

[74] **Johnson, R.A.,** 1988, Analytic nearest-neighbor model for fcc metals, Phys. Rev. B, 37, 3924.

[75] **Voter, A.F. and Chen, S.P.**, 1987, Accurate interatomic potentials for Ni, Al and Ni3Al, Mat. Res. Soc. Symp. Proc., Eds.: Siegel, R. W., Weertman, J. R., and Sinclair, R., MRS–82,175-180.

[76] **Mishin, Y., and Farkas, D.,** 1999, Interatomic potentials for monoatomic metals from experimental data and ab initio calculations, 5, 3393-3407.

[77] **Mishin, Y.,** 2004, Atomistic modeling of the γ and y' -phases of the Ni–Al system, Acta Materialia ,52, 1451–1467.

[78] http://www.ctcms.nist.gov/potentials/ : 20 Oct. 2016.

[79] http://www.grid.org.tr/ : 20 Oct. 2016

[80] http://www.ovito.org/ : 20 Oct. 2016.

[81] http://math.lbl.gov/voro++/ : 5 20 Oct. 2016.

Curriculum Vitae

Name/Surname : Nychir BAHRAM ABDULLAH

Contact Number : +905538037499, +9647504253595

Email Address : nechir.ak@gmail.com

Date of Birth : 21/03/1986

Place of Birth : **Iraq**-Ninawa

Education:

- BSc. Degree from University of Dohuk, College of Education/Zaxo, physics Department (2006-2010)

Work Field:

- Education (2011)

Scopes

- Molecular Dynamics Simulations, Computational Physics, Material Science.